V Mpampatsikos, ME Bressanelli, A Belleri, R Nascimbene. 2020. "A non-dimensional parametric approach for the design of PT tendons and mild steel dissipaters in precast rocking walls". Engineering Structures, Vol. 212 pp. 1-17. DOI: 10.1016/j.engstruct.2020.110513

Publisher's version at: https://doi.org/10.1016/j.engstruct.2020.110513

A non-dimensional parametric approach for the design of PT tendons and mild steel dissipaters in precast rocking walls

Vassilis Mpampatsikos[1,2], Michele Egidio Bressanelli[3], Andrea Belleri[4], Roberto Nascimbene[5]

Abstract

In recent years, important benefits for the seismic design of precast reinforced concrete wall structures have been obtained from the use of jointed wall-to-foundation connections, where gap openings are permitted, thus resulting in a rocking motion. The lumped rotation at the wall base protects the panels from damage, while gravity loads and unbounded post-tensioned (PT) tendons, designed to remain elastic, re-center the structure after an earthquake, thus solving the problem of residual displacements. External dissipaters, herein partially unbounded mild steel bars, limit the amplitude of lateral displacements providing the required dissipating capacity. The resulting response is characterized by flag-shaped hysteretic loops.

The paper investigates the parameters that may influence the design of rocking walls with supplemental energy dissipation devices in the form of mild reinforcing steel and aims to develop a parametric approach for the design of such systems. In this research, an analytical system of non-dimensional equations is developed for the design of PT tendons and dissipaters: location, area and prestressing force of the former, and location, area and unbounded length of the latter. A parametric approach suitable for the design practice is developed. This allows obtaining a simplified, quick, and accurate approach for the selection of PT tendons and energy dissipaters following a performance-based design approach. The procedure has been applied to a selected case study and validated by means of non-linear time history analyses.

Keywords: rocking wall; hybrid wall; post-tensioned tendons; mild steel dissipaters; displacement based design.

© 2020. This manuscript version is made available under the CC-BY-NC-ND 4.0 license http://creativecommons.org/licenses/by-nc-nd/4.0/

[1] PhD, structural Engineer, VMD Engineering s.r.l., Founding member, corso Indipendenza 1, 20129, Milano, Italy

[2] Contract professor, Politecnico di Milano, Department of Civil and Environmental Engineering, piazza Leonardo da Vinci 32, 20133, Milano, Italy

[3] PhD student, University of Bergamo, Department of Engineering and Applied Sciences, viale Marconi 5, 24044, Dalmine, Italy

[4] Associate professor, PhD, University of Bergamo, Department of Engineering and Applied Sciences, viale Marconi 5, 24044, Dalmine, Italy

Corresponding author: PH (+39)-035-2052007; FAX (+39)-035-2052040; email: andrea.belleri@unibg.it

[5] PhD, Head of the Head of the Building and Infrastructure Department, European Centre for Training and Research in Earthquake Engineering (EUCENTRE), Via Ferrata 1, 27100 Pavia, Italy

Introduction

Until the early nineties, the emulation of cast-in-place reinforced concrete (RC) buildings has been considered the most proper way to design precast concrete structures in seismic regions in order to provide communities with life-safe structures. The predominant idea was that a good structural system should accommodate large seismic demands by developing a nonlinear response at flexural plastic hinges distributed in pre-selected regions of the structure. Capacity design allowed to maximize the amount of energy dissipation and to reach a ductile behavior of the system.

In addition to life safety, another aspect to be accounted for in the design of earthquake proof buildings is resiliency (Cimellaro et al., 2010; REDI Rating system, 2013): the building should undergo limited and repairable damage after an earthquake with limited disruption to occupants while still being cost competitive compared to other solutions. One of the key differentiators of resilience-based design is preparedness for post-earthquake recovery to ensure continued operation and liveable conditions immediately after the earthquake. This led to the development of high-performance and low damage seismic resisting systems, such as base isolation and replaceable links lateral bracing (Mansour et al., 2008; Yin et al., 2019 among others), and to the consequent advancements in design methodologies. The first attempt to limit the seismic damage in precast prestressed concrete structures is represented by what proposed by Priestley and Tao (1993). They developed the idea of concentrating the ductility at the beam-column connections (jointed systems), in order to both control life-safety during strong ground motions and to reduce repair costs. Such systems are characterized by the so called "rocking response": all the rotation demand is lumped at the connections, where gap-openings are allowed. For this reason, they are referred to as "jointed rocking" systems. Unbounded post-tensioned (PT) tendons, designed to remain elastic during the earthquake, allow for re-centering. Although rocking walls without energy dissipaters present benefits in terms of reduction of residual displacements and protection of the structural members against damage, a pure rocking mechanism subjected to strong earthquakes may be characterized by high acceleration spikes as reported in shake table tests under realistic boundary conditions (Belleri et al., 2014) and to higher dispersion of the results (Twigden et al., 2019). An efficient solution to include energy dissipation in the main structural system was provided by the "jointed hybrid" systems developed in the PRESSS project (Priestley, 1996; Priestley et al., 1999), where mild steel bars or other additional external dissipative devices were adopted. These systems are referred to as "hybrid" because they match the restoring-force characteristics of jointed-rotating systems with the energy-dissipation characteristics of equivalent monolithic systems. The result is a center-oriented hysteretic response, governed by flag-shaped hysteretic loops (Restrepo and Rahman, 2007), where yielding of mild steel longitudinal reinforcement in tension and compression provides the required amount of dissipated energy (equivalent viscous damping ratios up to 28% according to Holden et al., 2003). This allows controlling and limiting both internal forces and deformations at ultimate limit state. Thus, according to this philosophy, the connections of the structural members rely on bonded mild steel reinforcement for strength, ductility capacity, energy dissipation and protection against possible brittle failures. Nonetheless, there are some issues with the possible failure of embedded dissipaters in hybrid wall systems, therefore solutions with spare mild steel dissipaters (Belleri et al., 2014) or external devices (Rodgers et al., 2007; Rodgers et al., 2008; Marriott et al., 2008; Marriott et al., 2011; Twigden et al., 2017; Golzar et al., 2017; Golzar et al., 2018) have been investigated. To further reduce the damage in the rocking wall system, it is possible to add steel plates/base channels (Belleri et al. 2014, Nazari et al., 2017) to confine the concrete toe region and therefore limiting the damage to the wall base. In addition, various researches have combined the use of a damage avoidance design philosophy together with rocking structures (Mander and Cheng, 1997; Ajrab et al., 2004; Hamid and Mander, 2010 and 2014).

In the case of cantilever precast walls detailed to behave as rocking/hybrid systems (Figure 1), the wall-foundation connection is made discontinuous in respect to concrete, while PT tendons ensure re-centering ability and provide the shear transfer mechanism, through shear friction or shear keys, at the joint level. Mild steel rebars anchored in the foundation and in the wall provide the required energy dissipation. The lateral displacements are accommodated by the development of a single joint opening at the wall-foundation interface. Figure 1 shows a comparison between monolithic and rocking/hybrid walls. In both cases, monolithic and rocking, the rotation demand is accommodated in the portion of the wall just above the foundation, while the rest of the wall is designed to avoid damage distribution along the wall height. For this scope, particular attention must be paid to protect the wall from further undesired hinging due to the amplification of the response caused by the higher mode effects. The concept of multi-rocking joints has also been investigated (Wiebe and Christopoulos, 2009).

Following the PRESSS project (Priestley, 1996; Priestley et al.,1999), a significant amount of analytical and numerical work was undertaken to better understand the behavior of unbounded post-tensioned precast wall systems to be used in seismic regions (Kurama et al., 1998a; Kurama et al., 1998b; Kurama et al., 1999; Kurama, 2000; Perez et al., 2003; Holden et al., 2003; Kurama 2005; Restrepo and Rahman, 2007; Mariott et al., 2008; Pennucci et al., 2009; Schoettler et al., 2009; Toranzo et al., 2009; Belleri et al., 2013; Belleri et al., 2014; Buddika and Wijeyewickrema, 2016; Qureshi and Warnitchai, 2016; Twigden et al., 2017; Twigden and Henry, 2019; Nazari et al., 2016). The response of hybrid rocking wall systems with externally mounted viscous dampers was also investigated (Kurama, 2000, Mariott et al., 2009).

While a significant amount of analytical research has been carried out, the majority of experimental tests on precast concrete rocking and hybrid walls have been conducted quasi-statically leading to performance-based design recommendations (Kurama, 2005; Restrepo and Rahman, 2007; Pérez et al., 2003; ACI ITG-5.1, 2008; ACI ITG-5.2, 2009). However, the performance of post-tensioned wall systems under dynamic conditions can only be addressed and confirmed through dynamic testing (Mariott et al., 2008, Schoettler et al., 2009, Toranzo et al., 2009, Nazari et al., 2016, Twigden and Henry, 2019) and design recommendations derived accordingly.

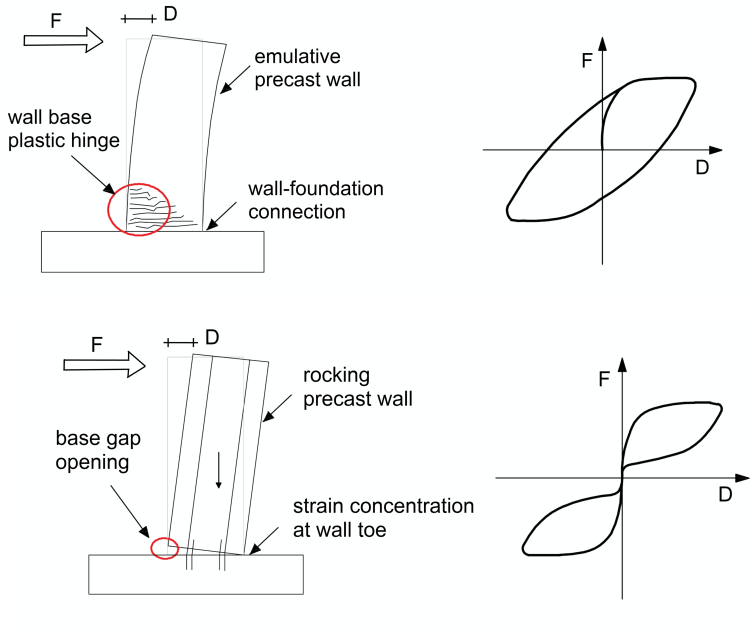

Figure 1. a) Equivalent monolithic response (RC emulative) of precast cantilever wall; b) jointed hybrid response

The present paper faces the need of practical guidelines for the design of hybrid wall systems, in particular the selection and location of PT tendons and mild steel dissipaters once the bending moment demand and displacement target are known. The principal target of this research is to develop numerical, analytical, graphic and conceptual tools for detailing the hybrid wall panel systems to satisfy the design requirements in terms of re-centering capability, bending moment capacity and target displacement. Although extensive parametric analyses have been conducted considering a wide variation of the dimensioning parameters, a comparison with the bounding values reported in ACI ITG-5.1 and ACI ITG-5.2 is also included. Furthermore, the research aims to follow a simplified approach for the design of such systems following a performance-based design procedure. The proposed design procedure is validated by means of nonlinear static and dynamic analysis on a reference case study showing its effectiveness.

Research significance

A non-dimensional parametric approach is herein adopted according to a performance-based design methodology, as an alternative to other design approaches for precast structures, such as the displacement-based design (Priestley et al., 2007; Belleri, 2017), or to other general approaches, such as the damage avoidance design philosophy (Hamid and Mander, 2014). The fundamental steps of the proposed approach are presented in Figure 2.

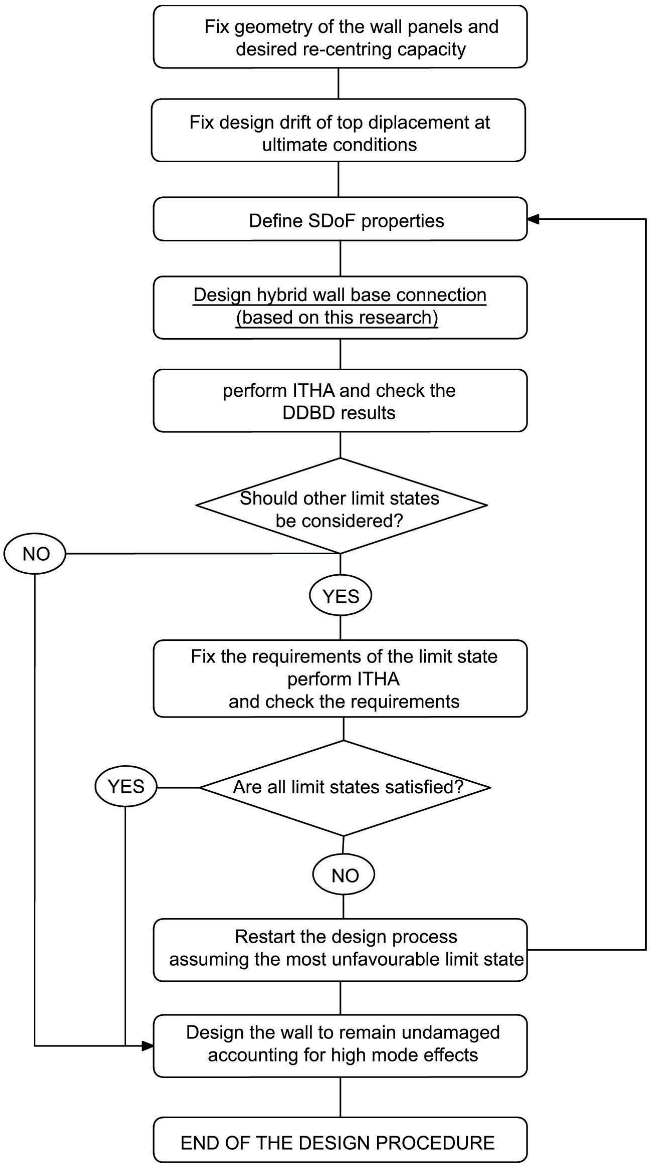

Figure 2. Fundamental step of the performance-based design procedure.

A description of each test is reported in the following.

i. Establish the maximum system drift angle under a seismic action corresponding to the design basis earthquake. ACI ITG-5.2 defines the maximum expected drift ratio for these wall systems equal to 3% and that the drift angle at the probable flexural capacity shall be equal or exceeding 1.5 times the drift at the design displacement;

ii. Select the desired re-centering capacity. ACI ITG-5.2 defines a minimum prestress force of PT tendons, $A_{PT}\cdot f_{se}+0.9\cdot D_c= A_d\cdot f_u$, and it states that the energy-dissipaters at the wall base shall provide at least 25% of the nominal flexural strength of the wall. Where f_{se} and A_{PT} are the effective stress and area in the PT tendons, respectively; f_u and A_d are the specified tensile strength and area of energy-dissipating reinforcement crossing the wall-foundation interface, respectively; D_c is the self-weight of wall plus any dead loads acting on it including the self-weight of components directly attached to the wall.

iii. Define the properties of an equivalent single degree of freedom system (SDOF).

iv. Design the wall-foundation rocking connection according to the procedure herein proposed.

v. Select a suitable set of natural accelerograms and perform inelastic time-history analyses (ITHA) to validate the consistency with the initial assumptions (design drift angle). The wall panels are modeled as elastic elements, with effective stiffness equal to the gross stiffness, since the rocking wall panels are designed to experience minor damage, even at ultimate limit state.

vi. Repeat steps i.–v. for other limit states. If the requirements corresponding to each limit state are satisfied, the design process is finished. It is worth mentioning that the amount and location of the PT tendons, as well the amount and position of the mild steel dissipaters are those determined at ultimate conditions.

vii. Finally, detail the wall panels to control damage (capacity design procedure) when subjected to the moment and shear distributions assessed at the ultimate limit state, considering the influence of higher modes as well.

Because the focus of the paper is the design of a hybrid system once the roof drift and the bending moment acting at the wall base have been defined, the procedure to obtain the SDOF parameters (i.e. the aforementioned point iii) is reported in the Appendix.

Parameters affecting the design

In hybrid wall systems, with partially unbounded mild steel dissipaters, the maximum displacements and strains need to be controlled and within acceptable bounds. The residual deformations are minimized by the re-centering contribution of PT tendons while the wall remains elastic and the shear sliding failure at the interface prevented (or minimized). During the design phase, the structure is detailed to reach the target lateral displacement before experiencing any failure mechanism, when subjected to the seismic action corresponding to the design basis earthquake and/or the maximum considered earthquake. This is a suitable method to control the rocking behavior of such systems. The design procedure practically reduces to the design of PT tendons and mild steel dissipaters at the wall-foundation rocking connection, which is the main source of lateral displacements. The wall reinforcement is determined subsequently, following capacity design, in order to provide enough resistance to limit the wall damage at ultimate conditions and enough confinement at the wall toes to accommodate the high concrete compressive strains arising at gap opening (Restrepo and Rahman, 2007; Belleri et al., 2014). Nevertheless, the wall slenderness and stiffness affect the outcome of the design procedure, i.e. the amount of PT tendons and dissipative devices. It emerges that the design of hybrid walls is much more complex than the design of monolithic cantilever walls. Moreover, unlike monolithic cantilever walls, hybrid systems allow controlling the amount of the hysteretic response through the calibration of the re-centering and dissipative capacities of the system, i.e. selecting properly the amount of PT tendons and dissipaters, respectively.

A series of design recommendations have been proposed in the past (among others: Kurama et al., 1999; Restrepo and Rahman, 2007; ACI ITG-5.1, 2008; Pennucci et al., 2009; ACI ITG-5.2, 2009; Belleri et al., 2014). In this research, in order to develop a more general and detailed discussion of the subject, an analytical system of non-dimensional equations is proposed. Before presenting the analytical equations, it is worth highlighting the governing parameters and unknowns. A complete list of symbols is reported at the end of the paper.

Design targets

- Design roof drift ratio (θ_{top}).
- Normalized design base bending moment, $\mu_M = M_b / (A_c \cdot f_c \cdot B)$, estimated following the equivalent SDOF substitute structure method developed by Shibata and Sozen (1976).

θ_{top} and M_b are known quantities during the design procedure.

Concrete properties

- Unconfined concrete (E_c, f_c, ε_{co}, ε_{cu})
- Confined concrete (Mander et al., 1988) (f_{cc}, ε_{cco}, ε_{ccu}). An appropriate confinement level must be assured to preserve the integrity of the concrete at wall toes (Restrepo and Rahman, 2007; Belleri et al., 2014.)

In general, the material properties are selected before performing the design process.

Wall properties

- Aspect ratio, H/B, generally determined through architectural considerations
- Ratio between the gap opening at wall base and the top drift ratio (θ_b/θ_{top}).
- Normalized neutral axis depth, $\zeta = c/B$, where c is the neutral axis depth.
- Normalized tributary axial load, $\nu = N/(A_c \cdot f_c)$.
- Ratio between the effective and the gross stiffness, γ_J. Twigden and Henry (2019), based on experimental tests and numerical studies, defined a value of the effective stiffness approximately equal to $0.6 \cdot I_g$, where I_g is the gross stiffness of the wall panel.

The variables θ_b/θ_{top} and ζ are the first two unknowns of the design problem;

PT tendons properties

- PT tendons steel properties (E_{PT}, f_{yPT}, ε_{PT}, $\gamma_{PT} \cdot f_{yPT}$). In particular, the PT tendons must remain elastic to assure a re-centering capacity of the wall. Thus, the maximum allowed stress, $f_{PT,\max}$, must not be larger than the yielding stress, f_{yPT}. Actually, in order to improve the safety of the structure, f_{PT} is recommended to be limited to a fraction of f_{yPT}, $f_{PT} \le \gamma_{PT} \cdot f_{yPT}$ since the yielding of PT tendons may lead to an increase of the lateral displacement and to a reduction of the re-centering action (Pérez et al., 2003; Restrepo et al, 2007). On the other hand, γ_{PT} should not be too small, as it would penalize excessively the performance of the wall. $0.9 \le \gamma_{PT} \le 1.0$ is a suitable range resulting from the parametric analyses, although, it is suggested to adopt γ_{PT} equal to 0.95 as recommended in ACI ITG-5.2.
- Normalized distance between the PT tendons ($D_{PTad} = D_{PT}/B$).
- Normalized length of the PT tendons ($L_{PTad} = L_{PT}/B$).Since the PT tendons are anchored at the foundations and at the top of the building, L_{PT} is approximately equal to H, by neglecting the embedded length of the tendons in the foundation. Using this approximation, we can adopt the following normalized length $L_{PTad} = H/B$.
- Mechanical ratio of the PT tendons, $\omega_{PT} = (A_{PT} \cdot f_{yPT})/(A_c \cdot f_c)$
- Ratio between the initial strain in the PT tendons and the yielding strain, $\varepsilon_{PTad} = \varepsilon_{PT}/\varepsilon_{yPT}$. ε_{PTad} is theoretically bounded by 0 and 1. Nevertheless, ε_{PTad} close to 0 and ε_{PTad} close to 1

are both not efficient solutions, as the former assigns the entire re-centering capacity to the contribution of the tributary gravity loads (no additional compressive force is transmitted to the wall), while the latter will force inelastic strain in the tendon due to rocking, therefore compromising the re-centering capacity of the system. Hence $\varepsilon_{PTad} = 0.5$ is generally assumed in this research.

D_{PTad} and ω_{PT} are the third and fourth unknowns of the design problem.

Dissipative devices properties

- Mild steel for dissipaters (E_d, f_{yd}, f_{ud}, ε_{yd}, ε_{ud}, $\varepsilon_{d,\max}$).
- Normalized distance between the dissipative devices ($D_{dad} = D_b / B$).
- Normalized unbounded length of the dissipative devices ($L_{dad} = L_b / B$).
- Mechanical ratio of the dissipative devices, $\omega_d = (A_d \cdot f_{yd})/(A_c \cdot f_c)$.

D_{dad}, L_{dad} and ω_d are the fifth, sixth, and seventh unknowns of the design problem.

Hysteretic shape

- Ratio between the re-centering, i.e. provided by the PT tendons and gravity loads, and the dissipative bending moments, i.e. provided by the dissipative devices, at design conditions, λ. Mpampatsikos et al. (2009) showed that λ at design conditions is slightly larger than the value ($\lambda_{\min}$) related to yielding of the dissipative devices. In particular, the ratio $\lambda_{\min} / \lambda$ varies from 1.04 (λ = 1) to 1.12 (λ = 3). Thus, in order to assure a re-centering capacity, $\lambda \geq 1.2$ is suggested, in agreement with Pampanin et al. (2001) who proposed $\lambda \geq 1.25$.

Non-dimensional system of equations

Six equations govern the design procedure. Three compatibility equations: Equation (1) for the wall compatibility deformation; Equation (2) for the PT tendons and Equation (3) for the dissipative devices (compatibility relations at jointed connection). Two equilibrium equations: Equation (4) for the vertical translational equilibrium and Equation (5) for the rotational equilibrium (or bending moment equilibrium). Equation (6) represents the ratio between the re-centering and the dissipative bending moments.

Assuming a bilinear shape of the mild steel $\sigma - \varepsilon$ curve, with hardening parameter $\mu_{Ed} = E_{pl,d} / E_{el,d}$, the following 6x6 system of equations is obtained. The interested reader is referred to Mpampatsikos (2009) for the derivation of such equations.

$$\theta_b = \theta_{top}\left[1 + \frac{4f_c}{\gamma_J E_c}\left(\frac{H}{B}\right)^2 \nu\right] - \frac{4f_c}{\gamma_J E_c}\frac{H}{B}\mu_M \tag{1}$$

$$D_{PTad} = \frac{2\left(\gamma_{PT}\varepsilon_{yPT} - \varepsilon_{PT}\right)L_{PTad}}{\theta_b} - 1 + 2\zeta \tag{2}$$

$$D_{dad} = \frac{2\varepsilon_{d,\max} L_{dad}}{\theta_b} - 1 + 2\zeta \tag{3}$$

$$\frac{1}{4}\omega_{PT}\frac{\theta_b \cdot D_{PTad}{}^2}{\varepsilon_{yPT}\cdot L_{PTad}} + \frac{1}{4}\omega_d \mu_{Ed}\frac{\theta_b \cdot D_{dad}{}^2}{\varepsilon_{yd}\cdot L_{dad}} + \alpha\zeta\left(0.5 - \beta\zeta\right) = \mu_M \tag{4}$$

$$\omega_{PT}\left[\frac{\varepsilon_{PT} + \theta_b\left(0.5-\zeta\right)/L_{PTad}}{\varepsilon_{yPT}}\right] + \omega_d\left[1 - \mu_{Ed}\left(1 - \frac{\theta_b\left(0.5-\zeta\right)/L_{dad}}{\varepsilon_{yd}}\right)\right] + \nu - \alpha\zeta = 0 \tag{5}$$

$$\lambda = \frac{\omega_{PT}\left\{\left(0.5-\beta\zeta\right)\left[\frac{\varepsilon_{PT} + \theta_b\left(0.5-\zeta\right)/L_{PTad}}{\varepsilon_{yPT}}\right] + \frac{1}{4}\frac{\theta_b \cdot D_{PTad}{}^2}{\varepsilon_{yPT}\cdot L_{PTad}}\right\} + \nu\left(0.5-\beta\zeta\right)}{\omega_d\left\{\left(0.5-\beta\zeta\right)\left[1 - \mu_{Ed}\left(1 - \frac{\theta_b\left(0.5-\zeta\right)/L_{dad}}{\varepsilon_{yd}}\right)\right] + \frac{1}{4}\mu_{Ed}\frac{\theta_b \cdot D_{dad}{}^2}{\varepsilon_{yd}\cdot L_{dad}}\right\}} \tag{6}$$

where α and β are the parameters needed to define the equivalent rectangular stress block for the compressed concrete. α and β account for: i) the confinement properties of the concrete core, ii) the unconfined properties of the concrete cover and iii) the actual $\sigma - \varepsilon$ curve of the concrete. Sensitivity analyses were conducted to establish appropriate α and β values, i.e. leading to neutral axis depths close to the real values for every allowed combination of the design parameters.

In particular, the compatibility equations at the controlled rocking section are not based on the well-known Navier-Bernoulli hypothesis of plane sections. In fact, such hypothesis is violated due to the presence of gap openings, unbounded PT tendons and partially unbounded mild steel dissipative bars.

Finally, since seven unknowns have been recognized (θ_b / θ_{top}, ζ, D_{PTad}, ω_{PT}, D_{dad}, L_{dad} and ω_d), one of them must be considered as an initial design choice. In this research, L_{dad} is generally assumed as a fixed parameter; nevertheless, any other choice would be permitted.

Suggested range of variability for the design parameters

In order to solve the above-described 6x6 problem (Equations 1 through 6), the ranges of the following quantities (θ_{top}, μ_M, ζ, λ, D_{PTad}, D_{dad}, H/B, ε_{PTad} and L_{dad}) need to be bounded by means of engineering considerations, in order to get significant results.

The hybrid walls with controlled rocking response at the wall-foundation interface are able to accommodate large displacements, with minor residual displacements. Small design displacements do not allow activating the dissipative devices. Nevertheless, too large displacements could be incompatible with wall-slab connections and integrity of non-structural elements. Examples of slotted wall-slab connections assuring vertical tolerances between the wall and the slab are reported in Schoettler et al. (2009) and in Belleri et al. (2014). For these reasons, in this research, the top drift angle is considered in the range 1.5%-3.0%.

Considering spectral shapes according with EN 1998-1 and a wide range of seismic intensity, tributary mass, wall slenderness and viscous damping ratios, Mpampatsikos (2009) showed that the normalized design base bending moment (μ_M), is bounded in the range 0-0.15.

The neutral axis depth, ζ, needs to be limited, as very large ζ can compromise the stability of the compressed chord of the wall. Restrepo and Rahman (2007) suggested that the neutral axis depth of the walls at the life safety performance objective should be limited to ensure hysteretic response stability and geometrical stability, at this regard a neutral axis ratio greater than 0.15 may result in the loss of initial stiffness due to concrete residual strains at the wall toes after reaching the design displacement. Perez et al. (2003) reported the sudden buckling and failure of a rocking wall exhibiting a neutral axis ratio of 0.3. In order to avoid this problem, they suggested limiting the neutral axis depth to 0.3. A value of 0.15 was also considered as the design objective of the DSDM project for the maximum considered earthquake (Schoettler et al., 2009; Belleri et al., 2014). Thus, for the proposed parametric procedure, an upper limit of 0.3 is recommended.

As already stated, a ratio between the re-centering and the dissipative bending moments at design conditions (λ) greater than 1.2 is suggested to avoid residual displacements. On the other hand, in order to assure enough dissipative capacity to maintain the maximum displacement below the design target, $\lambda \leq 3$ could be considered.

The efficiency of the PT tendons is affected by their mutual distance, which must be not too large. Moreover, a very large D_{PTad} reduces drastically the elastic strain, ε_{PT}, that can be applied. Thus, $0 \leq D_{PTad} \leq 0.6$ is recommended. Similarly, in the case of dissipaters, $0 \leq D_{dad} \leq 0.8$ is recommended to avoid an elastic response of the dissipater closer to the neutral axis.

In the following, it is shown that the normalized neutral axis depth (ζ) is almost independent from all the design variables but μ_M. In particular, for a first estimate of the system response $\mu_M \approx 0.5\zeta$ can be reasonably assumed.

Then, assuming $\theta_b \approx 0.95\theta_{top}$ (Mpampatsikos, 2009) and $\varepsilon_{PTad} = 0.5$, the compatibility condition of the PT tendons (Eq. 2) becomes:

$$D_{PTad} \approx 1.05\frac{\varepsilon_{yPT}\, H/B}{\theta_{top}} - 1 + 4\mu_M \tag{7}$$

Eq. 7 can be used as a first rough criterion for properly selecting the design parameters (H/B, θ_{top}, μ_M) in order to obtain significant D_{PTad} values. Eq. 7 is graphically represented in Figure 3 assuming the following values of the design parameters $2 \le H/B \le 4$, $0 \le \mu_M \le 0.15$ and $1.5\% \le \theta_{top} \le 3\%$. Such parameters are design choices.

The wall aspect ratio, H/B, should be large enough to avoid sliding shear failure at the wall-foundation interface. Restrepo and Rahman (2007) suggested:

$$\frac{H}{B} \ge \frac{\omega_d \cdot \omega_f}{2\mu_f} \tag{8}$$

Assuming $\mu_f = 0.7$ (Crisafulli et al., 2002), $\omega_d = 1.2$ (Fronteddu et al., 1998) and $\omega_f = 1.8$(Paulay and Priestley, 1992), Eq. 8 results in $H/B \ge 1.55$. Additional considerations on the shear friction under dynamic conditions of rocking and hybrid walls are reported in Belleri et al. (2014).

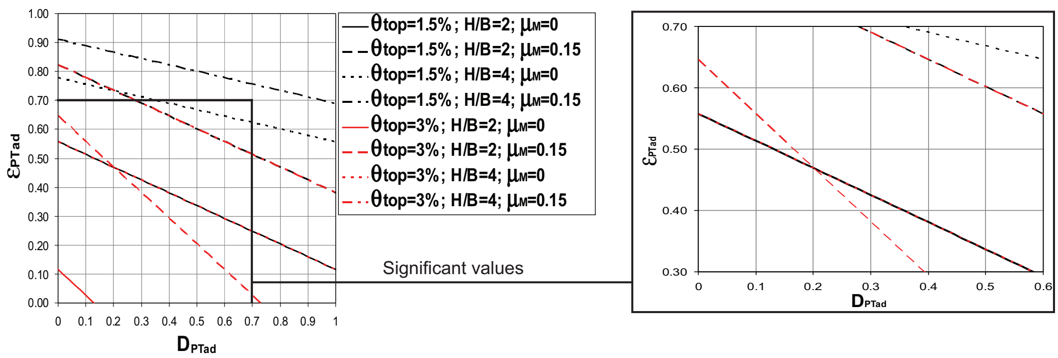

Figure 3. Significant values of D_{PTad} and ε_{PTad} where $0 \le D_{PTad} \le 0.6$ and $0.3 \le \varepsilon_{PTad} \le 0.7$ for different values of the selected design parameters, H/B, θ_{top}, and μ_M.

On the other hand, if H/B is too small, there will be not enough elastic strain, ε_{PT}, available at the design drift θ_{top}, therefore leading to premature yielding of PT tendons. In order to have $\varepsilon_{PT} > 0$ at the design drift θ_{top}, the following condition must be satisfied:

$$\frac{H}{B} > 0.475\frac{\theta_{top}}{\varepsilon_{yPT}}\left(1 + D_{PTad} - 2\zeta\right) \tag{9}$$

where for low-rise or medium-rise buildings θ_b has been reasonably approximated as $0.95\theta_{top}$ (Mpampatsikos, 2009).

Considering the following variability of the parameters $0 \le D_{PTad} \le 0.6$, $1.5\% \le \theta_{top} \le 3\%$ and assuming $\zeta = 0$ (lower bound) and $\varepsilon_{yPT} = 1450/180000$ it results in $1.77 \le H/B \le 2.83$. The lower bound of H/B is the higher value between Eq. 8 and Eq. 9. In this paper, $H/B \ge 2$ is considered. Since this research is not directly addressed to high-rise and slender buildings, the upper bound of H/B is limited to 4. Therefore, in this research, H/B is considered in the range $2 \le H/B \le 4$.

Theoretically, ε_{PTad} can vary between 0 and 1 as mentioned before and $\varepsilon_{PTad} = 0.5$ appears the best choice between the re-centering capacity and the available ε_{PT}. Nevertheless, both re-centering capacity and available ε_{PT} depend on D_{PTad} as well: the re-centering capacity increases if D_{PTad} increases, but the available ε_{PT} decreases, and vice-versa. Therefore $0.3 \le \varepsilon_{PTad} \le 0.7$ is considered in this research.

Considering the unbounded length of the mild steel dissipaters, L_{dad}, it is observed that in the case of a too large value the design gap opening will not be enough to force yielding in the mild steel dissipaters, therefore compromising the system energy dissipation. Assuming $\mu_M \approx 0.5\zeta$ and $\theta_b \approx 0.95\theta_{top}$, as obtained from the parametric analyses (Mpampatsikos, 2009) and shown in Figure 4(a) and (b), Eq. 3 becomes:

$$D_{dad} \approx 2.1\frac{\varepsilon_{d,\max} L_{dad}}{\theta_{top}} - 1 + 4\mu_M \tag{10}$$

or equivalently:

$$L_{dad} \approx 0.475\frac{\theta_{top}}{\varepsilon_{d,\max}}(1 + D_{add} - 4\mu_M) \tag{11}$$

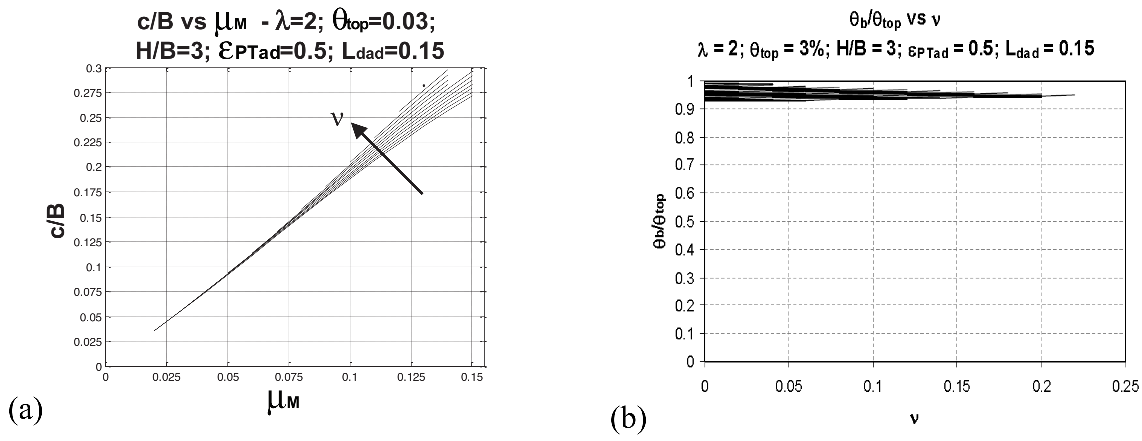

Figure 4. Variation of ζ=c/B as a function of μ_M (a), variation of $\vartheta_b/\vartheta_{top}$ as a function of ν for different μ_M (b).

Eq. 10 is graphically represented in Figure 5. The following values of the design parameters are considered: $0 \le \mu_M \le 0.15$, $1.5\% \le \theta_{top} \le 3\%$ and $\varepsilon_{d,\max} = 0.1$. The largest value of L_{dad} is obtained when D_{dad} and θ_{top} are both at maximum values ($D_{dad} = 0.8$ and $\theta_{top} = 3\%$) and μ_M tends to zero. Figure 5 shows that, in such conditions, L_{dad} is roughly equal to 0.26. The upper bound is a function of the maximum allowed mild steel strain, $\varepsilon_{d,\max}$. In this research $\varepsilon_{d,\max} = 0.1$ is assumed. If $\varepsilon_{d,\max} > 0.1$, the maximum L_{dad} will be smaller than 0.26 and vice versa. ACI ITG-5.2 suggests a development length in tension equal to 25 times the bar diameter.

Table 1 contains a summary of the suggested range of parameters.

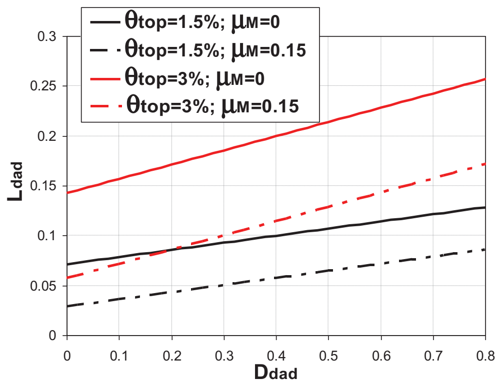

Figure 5. The normalized length of the dissipative devices vs. the normalized distance between the dissipative devices for different values of the selected design parameters θ_{top} and μ_M with $\varepsilon_{d,max} = 0.1$.

Table 1. Summary of the suggested range of parameters.

Parameters	H/B	θ_{top}	ζ	λ	ν	μ_M	D_{PTad}	D_{Dad}
Range	2÷4	1.5÷3%	0÷0.3	1.2÷3	0÷0.16	0÷0.15	0÷0.6	0÷0.8

Stress block parameters

The equations describing the stress-block parameters, α and β, should be added to the system of the equations previously presented. Although, in this research α and β are considered as known values to simplify the design procedure.

An extensive sensitivity analysis has been carried out. The following iterative procedure was followed until convergence (generally two iterations are enough): tentative values of α and β are assumed, the systems of non-dimensional equations is solved and the obtained solution is checked through a nonlinear static analysis using a fiber model approach (Spacone et al., 1996) extensively checked in previous researches (Brunesi and Nascimbene, 2014; Casotto et al., 2015; Nascimbene, 2015) using Opensees (2009) or Seismostruct (2015). This procedure was performed by varying the following design parameters one at a time: $0 \le \nu = N/(A_c \cdot f_c) \le 0.16$ in steps of 0.02, $0.01 \le \mu_M \le 0.15$ in steps of 0.01, $1.5\% \le \theta_{top} \le 3\%$ in steps of 0.0025, $2 \le H/B \le 4$ in steps of 0.25, $0.05 \le L_{dad} \le 0.25$ in steps of 0.05, and $1.25 \le \lambda \le 3$ in steps of 0.25. The obtained results confirm that α and β are rather insensitive to the variation of all design parameters but μ_M. Table 2 and Table 3 show the results and errors of each step of the iterative procedure, for $\mu_M = 0.05$ and $\mu_M = 0.1$, respectively. Analogous results are obtained for each value of μ_M. Although both α and β increase monotonically with μ_M, it is herein suggested to consider their mean values, $\alpha_{mean} = 1.22$ and $\beta_{mean} = 0.48$. The sensitivity analysis shows that an error less than 3% is obtained in all the cases when a proper concrete confinement at the wall base is selected, thus validating the simplified approach.

Table 2. Iterative procedure for α and β (solution of the system with μ_M =0.05)

Note: errors percentage in brackets

VALUES	α	β	ζ	ω_d	ω_{PT}	D_{dad}	D_{PTad}
Starting Values	1.164	0.443	0.093	0.0277	0.0136	0.208	0.177
1st Iteration	1.210 (-4.02)	0.467 (-5.37)	0.088 (3.98)	0.0277 (-0.03)	0.0137 (-0.59)	0.201 (3.55)	0.170 (4.19)
2nd Iteration	1.213 (-0.24)	0.468 (-0.20)	0.089 (0.24)	0.0277 (0.01)	0.0137 (0.04)	0.200 (0.21)	0.170 (0.25)
Convergence reached	1.213 (-0.01)	0.468 (-0.01)	0.089 (0.00)	0.0277 (0.00)	0.0137 (0.00)	0.200 (0.00)	0.170 (0.00)

Table 3. Iterative procedure for α and β (solution of the system with μ_M =0.10)

Note: errors percentage in brackets

VALUES	α	β	ζ	ω_d	ω_{PT}	D_{dad}	D_{PTad}
Starting Values	1.164	0.443	0.194	0.0621	0.112	0.434	0.403
1st Iteration	1.222	0.491	0.188	0.0631	0.115	0.423	0.391
	(-5.77)	(-10.64)	(4.02)	(-1.47)	(-2.26)	(3.57)	(3.86)
2nd Iteration	1.234	0.495	0.186	0.0631	0.115	0.419	0.388
	(-1.26)	(-1.05)	(0.87)	(-0.02)	(-0.03)	(0.77)	(0.83)
Convergence reached	1.235	0.496	-	-	-	-	-
	(-0.07)	(-0.09)	(0.00)	(0.00)	(0.00)	(0.00)	(0.00)

Numerical solution of the parametric design problem

In this section, an attempt to decouple the non-dimensional equations (Eq. 1 through Eq. 6) is developed to simplify the design procedure. First, θ_b / θ_{top} can be computed directly from Eq. 1, since the right-hand-side does not include any unknown variable. D_{PTad} and D_{dad} (Eq. 2 and Eq. 3, respectively) cannot be computed as long as ζ remains unknown. Unfortunately, ζ requires the solution of the complete system of equations. Such approach is not seen suitable for the design practice. An attempt to calibrate a numerical expression for ζ is provided in the following. Given ζ, Eq. 2 and Eq. 3 provides directly D_{PTad} and D_{dad}. ω_d and ω_{PT} are obtained solving the system of two equations chosen among Eq. 4, Eq. 5 and Eq. 6. Figure 6 shows the mechanical ratio of mild steel dissipative devices, ω_d, versus the normalized base bending moment capacity, μ_M.

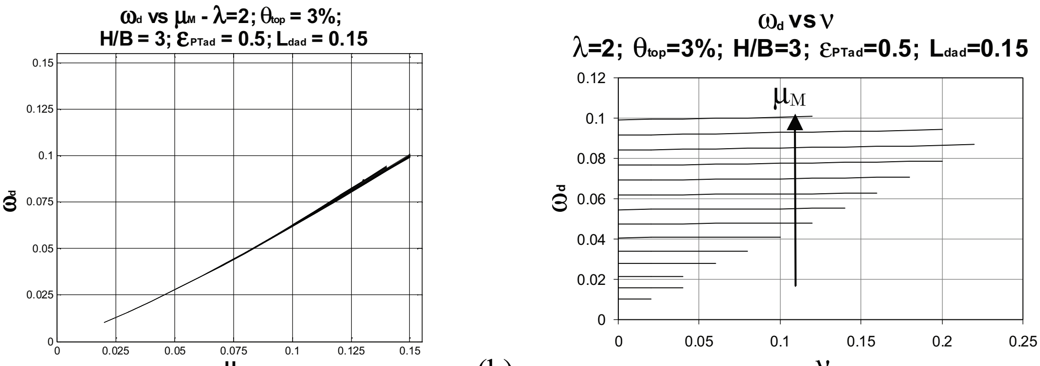

(a) (b)

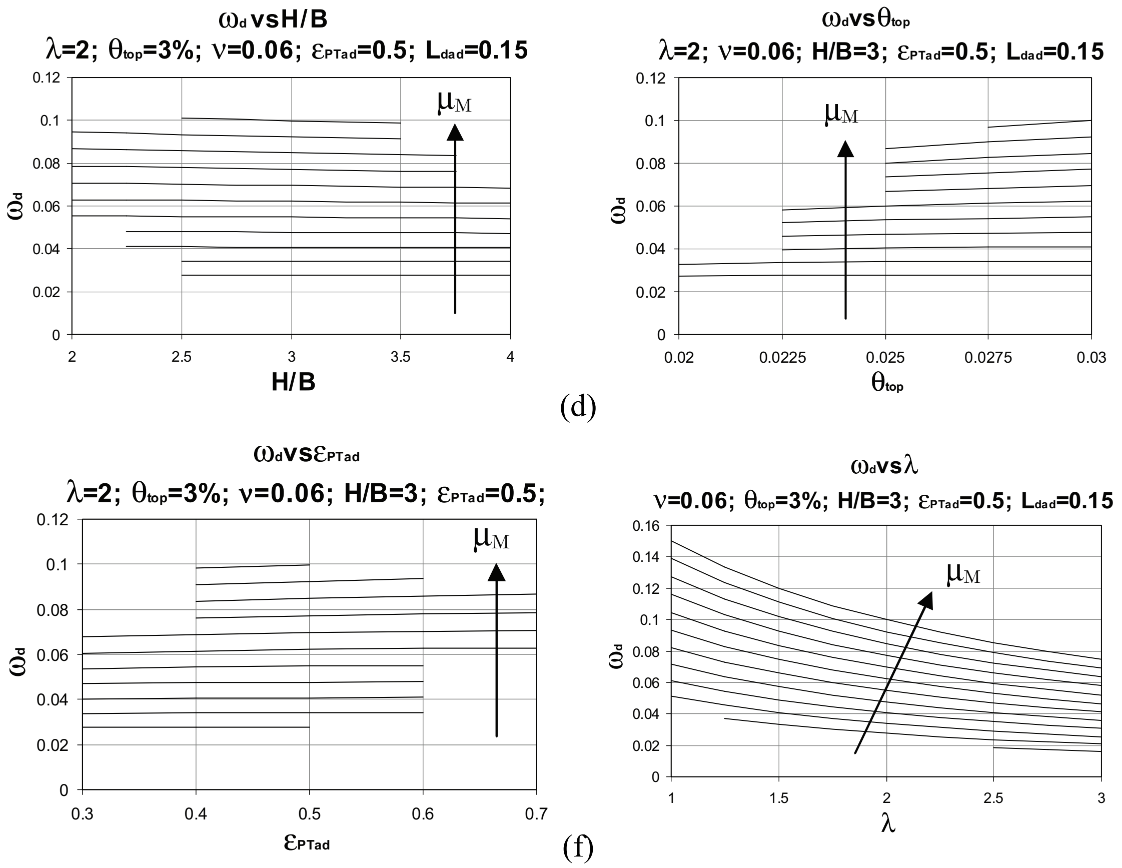

(c) (d)

(e) (f)

Figure 6. The mechanical ratio of mild steel dissipative devices vs. the normalized base bending moment capacity (a) and vs. the normalized axial load due to gravity loads (b); by fixing the normalized design base bending moment and the normalized axial load, no variation of ω_d (c) and θ_{top} (d) is appreciated by modifying the wall aspect ratio, *H/B*.; ω_d is insensitive to the variability of the normalized imposed strain of the tendons (e) but increases sensibly when λ decreases (f).

The influence of each parameter is investigated by changing one parameter at a time (ν, *H/B*, θ_{top}, ε_{PTad}, λ). It is evident that ω_d is a function only of μ_M and λ, while the other parameters determine negligible variations. Therefore, in the next section a numerical expression for ω_d is presented. Finally, ω_{PT} can be computed from either Eq. 4, Eq. 5 or Eq. 6. The results presented herein allow substituting the unpractical system of non-dimensional equations into six uncoupled equations, thus reducing drastically the complexity of the design process.

Calibration of the numerical expression for the non-dimensional neutral axis depth

Figures 7(a) illustrate ζ versus μ_M, for different ν, being all the other design parameters fixed. Both graphs show that ζ increases almost linearly with μ_M. Figures 7(b) and (c) show that, given μ_M and ν, a small increase of ζ is observed when H/B decreases and θ_{top} increases, respectively. Both trends are more pronounced for large μ_M, while ζ tends to be insensitive to H/B and θ_{top} as μ_M reduces. Figures 6(d) and (e) show that ζ is almost insensitive to the variability of λ and L_{dad}, respectively. In the light of these considerations, it can be concluded that ζ is mainly a function of μ_M; ν, H/B and θ_{top} represent secondary parameters. In particular, the relationship ζ - μ_M is fairly linear and passes through the origin. Varying all the parameters one at a time, the slope of $\zeta(\mu_M)$ changes, leading to a fan-shape set of curves. The variation of the slope is a function of the values of the other parameters. This is a proof that ζ cannot be expressed as the sum of different functions, but it should be calibrated through a single function of all the considered parameters:

$$\zeta = f(\mu_M, \nu, \frac{H}{B}, \theta_{top}) \tag{14}$$

The following power function is investigated:

$$\zeta = a \cdot \mu_M^b \tag{15}$$

where $a = a(\nu, H/B, \theta_{top})$ and $b = b(\nu, H/B, \theta_{top})$. For each combination of $0 \le \nu \le 0.30$ in steps of 0.02, $1.5\% \le \theta_{top} \le 3\%$ in steps 0.0025, $2 \le H/B \le 4$ in steps of 0.25, the system of non-dimensional equations is solved varying μ_M from zero to 0.15, in steps of 0.01. Thus, 15 sets of data are obtained and fitted through the power function, using the least squares technique. In all cases the value of b is in the range $0.98 < b < 1.02$, indicating that a linear relationship can be assumed. Therefore, only the parameter a needs to be calibrated ($\zeta = a \cdot \mu_M$). The following formula is obtained:

$$\zeta = \left(\left(\left(4.726 - 133.1\theta_{top} \right) \frac{H}{B} + 269.2\theta_{top} - 8.957 \right) \nu + \left(0.3105\theta_{top} - 0.1992 \right) \frac{H}{B} + 25.08\theta_{top} + 1.666 \right) \mu_M \tag{16}$$

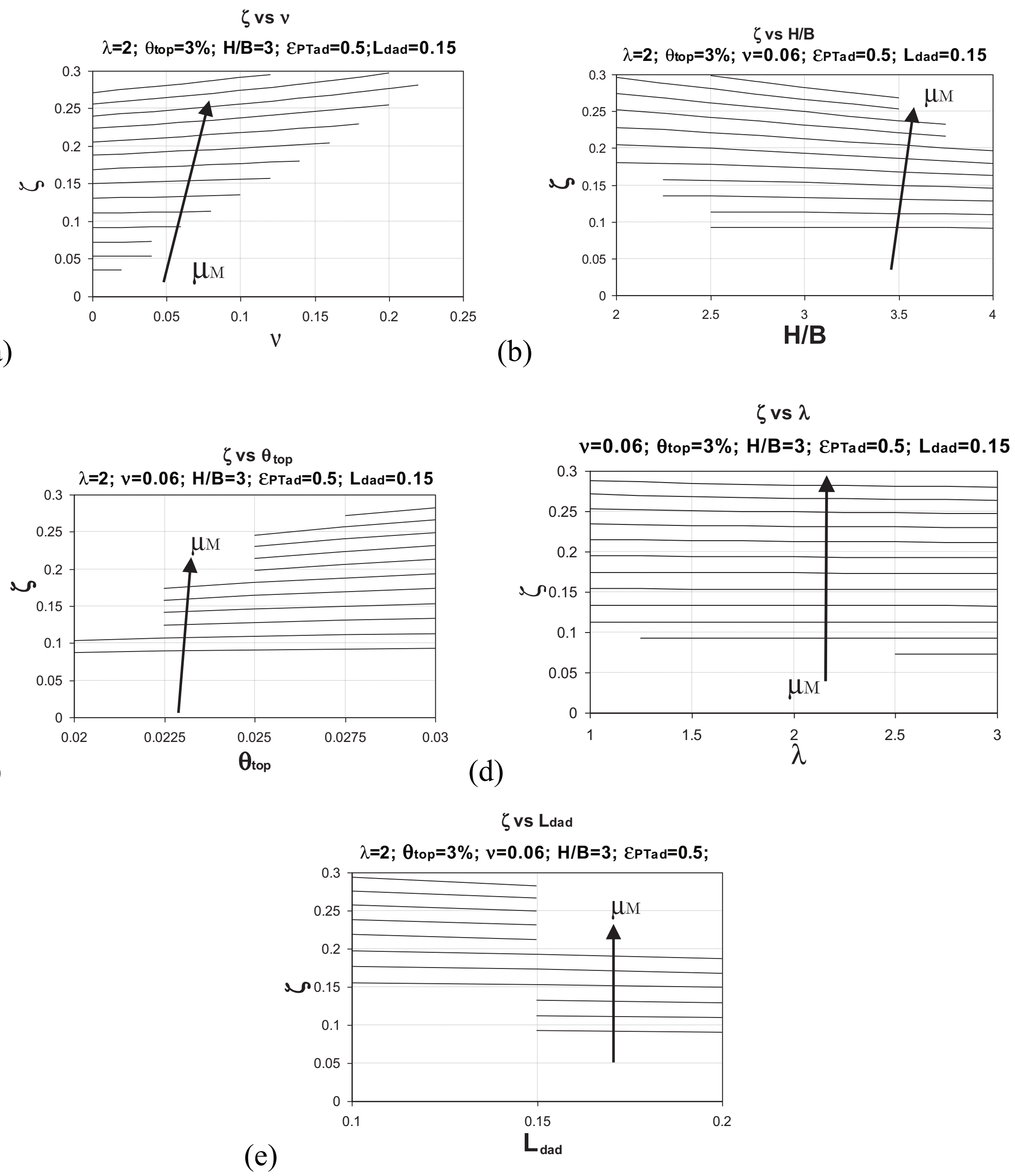

Figure 7. Variation of $\zeta = c/B$ as a function of: (a) μ_M ; (b) ν ; (c) aspect ratio, H/B ; (d) design top drift ratio; (e) λ ; (f) normalized length of the dissipative devices $L_{dad} = L_b/B$.

Figure 8 shows the comparison between ζ obtained from the system of equations (Eq. 1 through Eq. 6) and Eq. 16. The graphs prove the reliability of the proposed simplified assessment. It is worth mentioning that the error is smaller than 1% for every allowed combination of the design parameters.

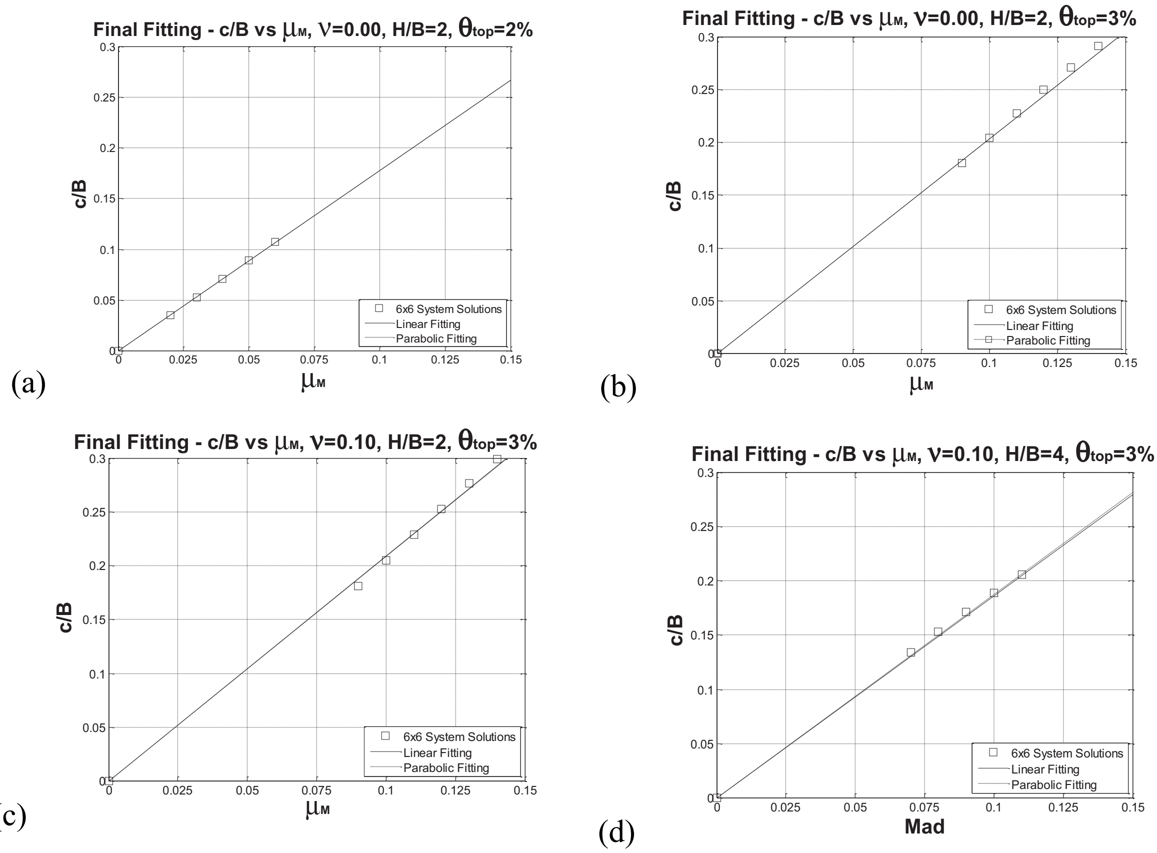

Figure 8. Comparison between the values of ζ obtained from solving the system of equations (Eq. 1 through Eq. 6) and the values obtained from Eq. 16 for different values of ν , H/B and θ_{top}.

Calibration of the numerical expression for the mechanical ratio of dissipaters

Figure 6(b) shows ω_d versus μ_M for different ν, being all the other design parameters fixed. It emerges that ω_d increases more than linearly with μ_M, while it is almost insensitive to ν. Figure 6(f) shows that ω_d increases sensibly when λ decreases. The ω_d - λ relationship seems to be inversely proportional. Figures 6(c), 6(d) and Figure 9 show that ω_d is not affected by H/B , θ_{top} and L_{dad} respectively.

It can be concluded that ω_d is mainly a function of μ_M and secondarily of λ. Three different functions are proposed to fit the results of the system of equations: i) linear function, $\omega_d = a \cdot \mu_M$, with one coefficient to calibrate; ii) parabolic function, $\omega_d = a \cdot \mu_M^2 + b \cdot \mu_M$, with two coefficients to calibrate; iii) power function, $\omega_d = a \cdot \mu_M^b$, with two coefficients to calibrate. For all the functions $a = a(\lambda)$ and $b = b(\lambda)$ are dependent on λ. Firstly, estimates for ω_d are obtained from the analytical system (Eq. 1 – Eq. 6), considering $0 \le \mu_M \le 0.15$ in steps of 0.01 and $1.25 \le \lambda \le 3$ in steps of 0.25. Since ω_d is sensitive only to μ_M and λ, the other parameters are fixed arbitrarily.

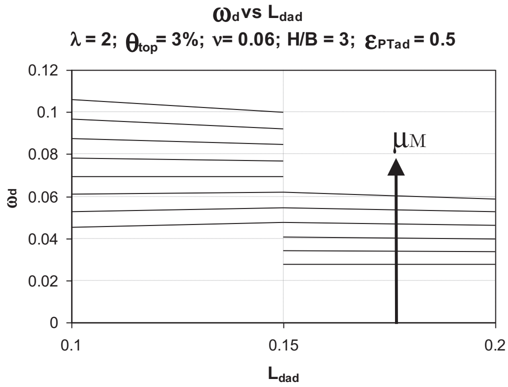

Figure 9. Variation of ω_d as a function of L_{dad}.

Then, the obtained values are compared to those found fitting the data through the linear, parabolic and power functions, using the least squares technique (Figure 10): a is assumed inversely proportional to λ in all the functions, while b is assumed inversely proportional to λ in the parabolic fitting and roughly constant in the power fitting. The resulting equations are:

$$\omega_d = \frac{1.806}{\lambda + 1.008}\mu_M \tag{17}$$

$$\omega_d = \frac{1.714}{\lambda + 0.6806}\mu_M^2 + \frac{1.604}{\lambda + 1.032}\mu_M \tag{18}$$

$$\omega_d = \frac{2.201}{\lambda + 0.9515}\mu_M^{(1.102 - 0.002267\cdot\lambda)} \tag{19}$$

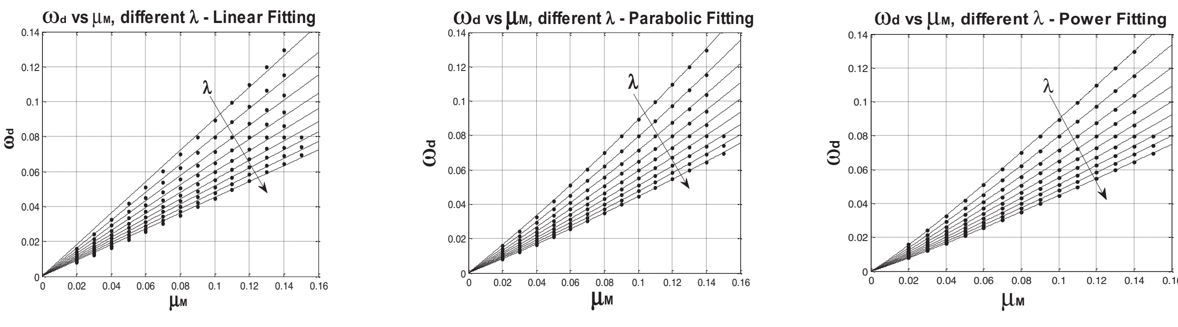

Figure 10. Comparison of values found by fitting the data through the linear, parabolic and power functions, using the least squares technique.

Figure 11 shows, for λ = 1.25 and 3, the comparisons between ω_d found from the analytical system of equations and the results of Eq. 17, Eq. 18, and Eq. 19. Graphically, it can be observed that both Eq. 18 and Eq. 19 furnish a very accurate estimate of the data obtained from the analytical system. The linear fitting is less accurate but still reaches a quite good prediction of ω_d. The maximum differences, $\Delta\omega_{d,\max}$, between the approximated (Eq. 17, Eq. 18, and Eq. 19) and the analytical solution are respectively: $\Delta\omega_{d,\max} = 3.8 \cdot 10^{-3}$, $\Delta\omega_{d,\max} = 7.5 \cdot 10^{-4}$ and $\Delta\omega_{d,\max} = 5.1 \cdot 10^{-4}$. The linear fitting is characterized by one order of precision less than the other solutions. Considering that both parabolic and power functions are characterized by the same degree of complexity, the power function (Eq. 19) is suggested for the design process. Figure 12 shows the simplified procedure formulas adopted for the design example.

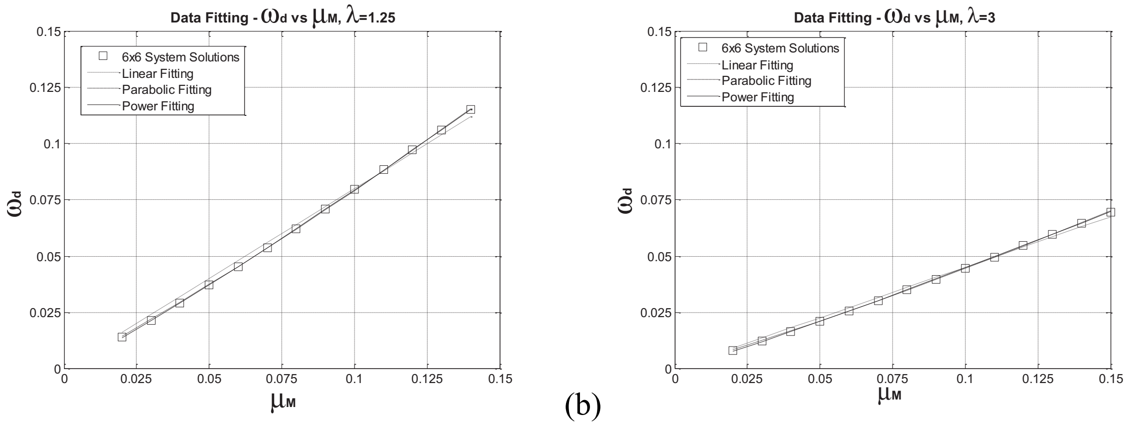

(a) (b)

Figure 11. Comparisons between ω_d found from the analytical system of equations (1)-(6), the linear fitting (17), the parabolic fitting (18) and the power fitting (19).

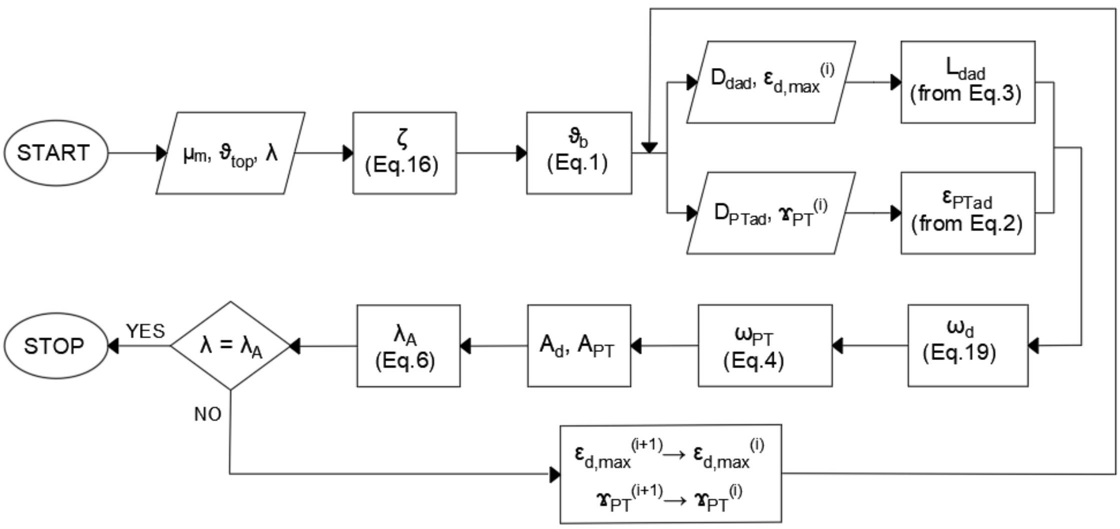

Figure 12. Simplified procedure adopted for design.

Design example

A case study is selected to validate the proposed procedure. The reference structure is a 5 storey building located in a European site with high seismicity: design spectrum corresponding to the life safety limit state in accordance to Eurocode 8 (CEN 2004) with soil class C and ground acceleration on rock a_g equal to 0.261g. The building height is 15m and the plan dimensions are 18m x 12m. Precast hybrid walls with mild steel dissipaters provide the lateral force resisting system.

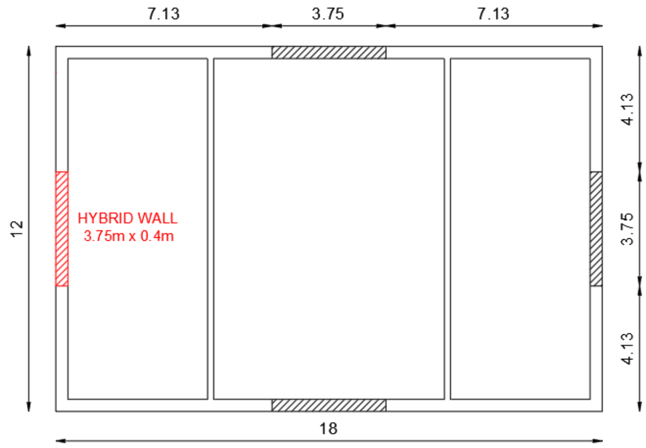

Figure 13. Schematic plan view of the structure. Note: dimensions in m.

For demonstration purposes, a single hybrid wall is analyzed in the following (Figure 13). The wall is 15m high and 3.75m wide, i.e. H/B equal to 4, and is characterized by concrete with cylindrical strength equal to 50MPa, steel reinforcement with yield strength equal to 455MPa and post tensioning (PT) tendons with nominal tensile strength equal to 1860MPa. The wall hysteretic form is defined as the relationship between re-centering capacity and design moment of the dissipative devices; at this regard a value of λ equal to 3 is selected. The longitudinal reinforcement ratio in the unconfined region is equal to ρ_l=0.3%, corresponding to 20 16mm diameter bars (A_s=40.21 cm^2), while in the transverse direction the reinforcement ratio is equal to ρ_t=0.3%. In the confined region the longitudinal reinforcement ratio is equal to ρ_l=1.3%, corresponding to 12 20mm diameter bars (A_s=37.70 cm^2). Figure 14 shows the main parameters of the wall cross-section involved in the design procedure.

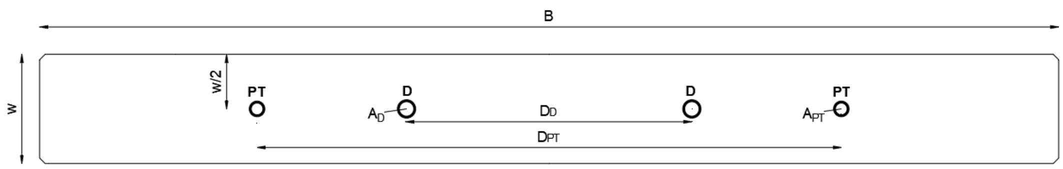

Figure 14. Cross-section of precast hybrid wall with indicated the main parameters.

Once the main geometrical features of the hybrid wall and the target design parameter (i.e. the roof drift, θ_{top}, herein taken as 1.5%) have been defined, it is possible to obtain the equivalent elastic SDOF system from the procedure presented in the Appendix. The results are reported in the following Table 4. From θ_{top} equal to 1.5% and μ_M equal to 0.025, it is possible to apply the proposed wall design procedure following the iterative process schematically represented in Figure 12.

Table 4. Summary of the results of the simplified procedure.

Design Parameter	Description	Value
μ_M	Normalized base bending moment	0.0205
μ_D	Displacement ductility	9.4
ξ_e	Equivalent viscous damping ratio of the substitute SDOF system	12.7 %
T_e	Equivalent period of the substitute SDOF system	1.9 s
M_e	Equivalent mass of the substitute SDOF system	379964 kg
K_e	Equivalent stiffness of the substitute SDOF system	4354 kN/m
V_b	Design base shear	720 kN
M_b	Design base moment	7900 kNm

In the first step, the neutral axis depth ζ is calculated with Eq. 16 (ζ = 0.03). At this point, it is possible to calculate the gap opening at the wall base with Eq. 1, considering θ_{top} equal to 1.5% as a design choice and γ_j=0.6 (Twigden and Henry, 2019). The normalized tributary axial load (ν) for the considered case study is 0.0065. This leads to a gap opening at the wall base ϑ_b (Eq. 1) equal to 1.4%.

Now, choosing the value of D_{PTad} and D_{Dad} equal to 0.44 and 0.16 respectively, from Eq. 2 it is possible to derive the initial strain in the PT tendons:

$$\varepsilon_{PT} = \gamma_{PT}\varepsilon_{yPT} - \left[\frac{\theta_b\left(1+D_{PTad}-2\zeta\right)}{2L_{PTad}}\right] = 0.514\% \tag{20}$$

Where $\varepsilon_{PT} = \varepsilon_{PTad}$ x ε_{yPT}, therefore ε_{PTad} is equal to 0.6, and γ_{PT} is 0.9. From Eq. 3, it is possible to derive the normalized unbounded length of the dissipative devices ($\varepsilon_{d,max}$=0.1):

$$L_{dad} = \frac{\theta_b\left(1+D_{Dad}-2\zeta\right)}{2\varepsilon_{d,\max}} = 0.08 \tag{21}$$

The distance D_{PT} of the PT tendons, the distance D_D of the dissipative devices and the length L_D of the dissipative devices are obtained from multiplying the previous dimensionless values times the wall width (B =3750mm), leading to 1650mm, 600mm and 290mm, respectively. The normalized length of the PT tendons, L_{PTad}, is approximately equal to H_{wall}/B = 4.

ω_d is calculated using the simplified formula (Eq. 19):

$$\omega_d = \frac{2.201}{\lambda + 0.9515} \mu_M^{(1.102-0.002267\lambda)} = 0.0098 \tag{22}$$

ω_{PT} is obtained from Eq. 5:

$$\omega_{PT} = \frac{\alpha\zeta - \nu - \omega_d \left[1 - \mu_{Ed} \left(1 - \frac{\theta_b (0.5-\zeta)/L_{dad}}{\varepsilon_{yd}} \right) \right]}{\frac{\varepsilon_{PT} + \theta_b (0.5-\zeta)/L_{PTad}}{\varepsilon_{yPT}}} = 0.024 \tag{23}$$

Subsequently, the re-centering capacity is validated by means of Eq. 6:

$$\lambda_A = \frac{\omega_{PT} \left\{ (0.5-\beta\zeta) \left[\frac{\varepsilon_{PT} + \theta_b (0.5-\zeta)/L_{PTad}}{\varepsilon_{yPT}} \right] + \frac{1}{4} \frac{\theta_b \cdot D_{PTad}^2}{\varepsilon_{yPT} . L_{PTad}} \right\} + \nu (0.5-\beta\zeta)}{\omega_d \left\{ (0.5-\beta\zeta) \left[1 - \mu_{Ed} \left(1 - \frac{\theta_b (0.5-\zeta)/L_{dad}}{\varepsilon_{yd}} \right) \right] + \frac{1}{4} \mu_{Ed} \frac{\theta_b \cdot D_{dad}^2}{\varepsilon_{yd} . L_{dad}} \right\}} = 3.3 \tag{24}$$

In the case λ_A is close enough to the initially assumed λ value it is possible to continue the procedure otherwise iterations are required.

The required area of PT steel tendons and dissipative devices are respectively:

$$\omega_{PT} = \frac{A_{PT} f_{yPT}}{A_c f_c} \rightarrow A_{PT-i} = \left(\frac{\omega_{PT}(A_c f_c)}{f_{yPT}} \right) /2 = 650\ mm^2 \tag{25}$$

$$\omega_d = \frac{A_d f_{yd}}{A_c f_c} \rightarrow A_{d-i} = \left(\frac{\omega_d(A_c f_c)}{f_{yd}} \right) /2 = 990\ mm^2 \tag{26}$$

Where A_c is the wall cross-section area. Therefore, a total of 7 tendons with 12.5mm diameter ($A_{PT-i-eff}$=651mm^2) and 2 mild steel dissipaters with 26mm diameter ($A_{d-i-eff}$=1060mm^2) per side are selected. The final wall properties are reported in Table 5.

Table 5. Summary of the wall properties.

Design Parameter	Description	Value
B	Base of the wall	3750 mm
w	Width of the wall	400 mm
H_f	Interstory height	3000 mm
H_T	Total height of the wall	15000 mm
θ_{top}	Design top drift	1.5 %
f_{cm}	Mean compressive strength of the concrete	58 MPa
E_c	Elastic modulus of the concrete	37278 MPa
ν	Normalized tributary axial load	0.0065
ψ	Normalized equivalent mass	0.0428
f_{yPT}	Yielding stress of the PT tendons	1634 MPa
f_{PTmax}	Maximum allowed stress of the PT tendons	1471 MPa
E_{PT}	Elastic modulus of the PT tendons	195000 MPa
ε_{yPT}	Yielding strain of the PT tendons	0.84%
ε_{PT}	Initial strain of the PT tendons	0.50%
L_{PT}	Length of the PT tendons	15000 mm
D_{PT}	Distance between the PT tendons	1650 mm
ε_{yd}	Yielding deformation of the dissipaters	0.22%
$\varepsilon_{d\text{-}max}$	Maximum strain of the dissipaters	0.1
f_{yd}	Yielding stress of the dissipaters	430 MPa
L_d	Length of the dissipaters	290 mm
D_d	Distance between the dissipaters	600 mm
μ_{ED}	Hardening parameter of the dissipaters	0.01

In order to evaluate the wall performance under seismic conditions, a finite element model has been defined with the professional software Midas Gen (2017) following the modeling suggestions contained in Belleri et al. (2013). Figure 15 shows the scheme of the considered finite element model. The wall is modeled with fiber elements. At the base, a short fiber element (4cm long) with a cross section characterized by a no-tension concrete material is placed to model the base gap opening. The PT tendons and the dissipaters are modeled with truss elements with non-linear properties, in particular fiber elements with Park hysteresis (Kent and Park, 1971) are considered. The pretension of the PT cables is applied by imposing a vertical displacement at each PT cable base corresponding to the pretension strain ($D_z = \varepsilon_{PT} \cdot L_{PT} = 75.45\, mm$). The connections between the wall and the tendons and between the wall and the dissipaters are made by rigid elements. The tributary floor mass is lumped at the wall at each floor level (m_x=94700kg for intermediate floors and m_x=89400kg for the top floor).

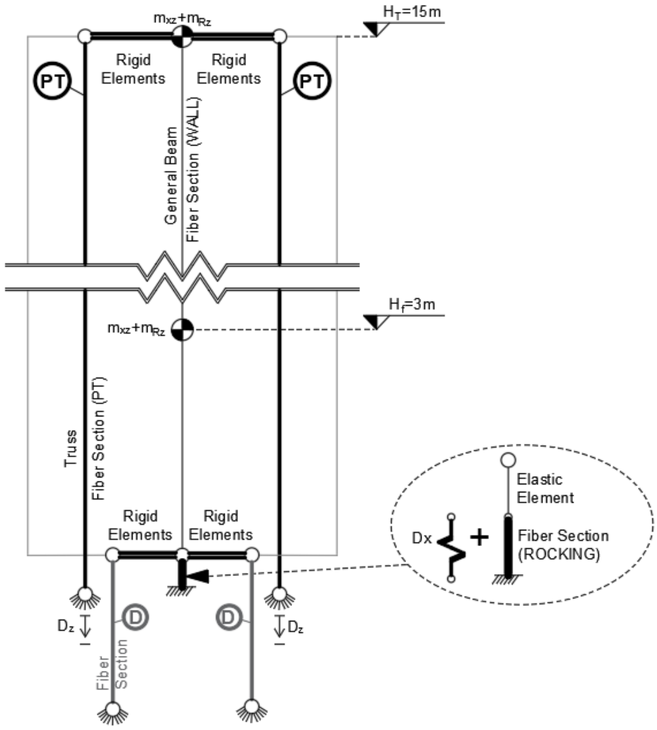

Figure 15. Schematic view of the finite element model of hybrid precast wall.

Note: PT represents the post-tensioning tendons; D represents the dissipaters

Figure 16 shows the results of a non-linear static analysis both in terms of base shear versus roof drift and in terms of base moment versus gap opening at the base. The results highlight the dissipative and re-centering behavior of the precast hybrid wall.

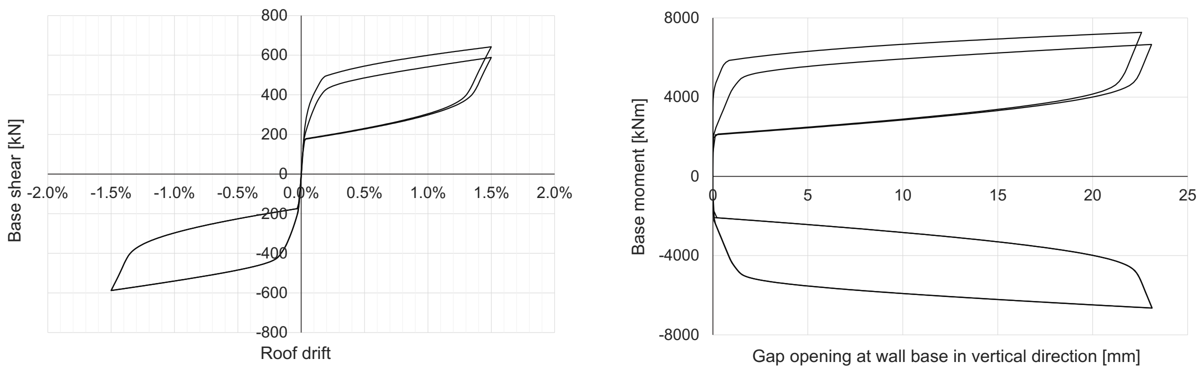

Figure 16. Results of non-linear static analyses in terms of base shear versus roof drift (left side) and base moment versus gap opening at the base (right side).

Non-linear time history analyses are conducted for various limit states: immediate occupancy limit state (IO) with a_g=0.079g, serviceability limit state, (S) with a_g=0.104g, life safety limit state (LS) with a_g=0.261g, and collapse prevention (CP) with a_g=0.334g. Three spectrum-compatible ground motions are defined for each limit state by means of the SIMQKE algorithm (Venmarcke and Gasparini 1976) with a stationary part of 15s and an overall duration of 25s. Mass and tangent stiffness proportional Rayleigh damping is applied for all the analyses with relative damping equal to 3% (Kurama, 2000; Kurama, 2002; Twigden and Henry, 2019) for the periods 0.3s and 2.0s. The results of the most demanding ground motion per limit states are reported in the following. Figure 17 shows the results of the analysis in terms of base moment versus base rotation for the various limit states, while Figure 18 shows the maximum inter-story drift ratio at each floor. It is worth noting that there are no residual displacements and that the design procedure succeeded in controlling the inter-story drift for the life safety limit state as required: generally, the maximum drift at the life safety level is lower than the design value of 1.5% leading to conservative mean results, as also reported in Twigden and Henry (2019). Figure 19 shows the bending moment envelope at each floor.

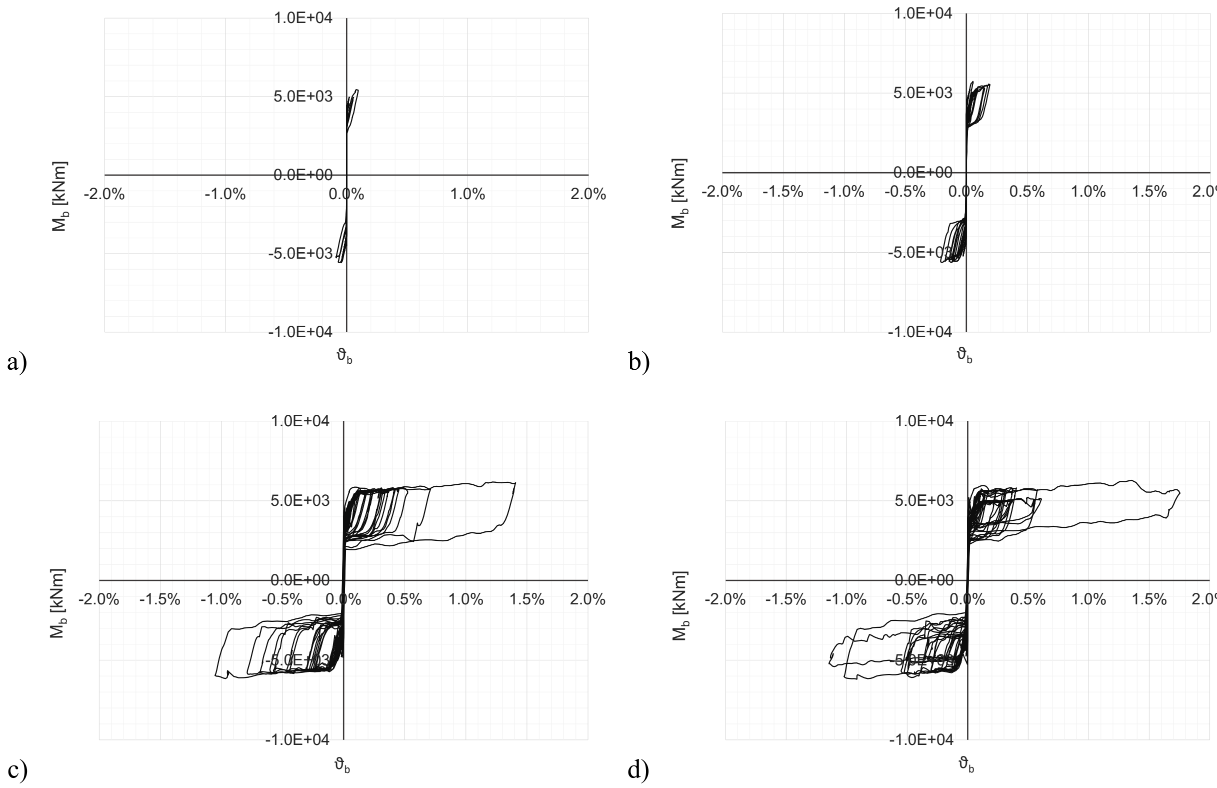

Figure 17. Results of time history analysis in terms of base moment M_b versus base rotation ϑ_b for immediate occupancy limit state (a), serviceability limit state (b), life safety limit state (c) and collapse prevention (d).

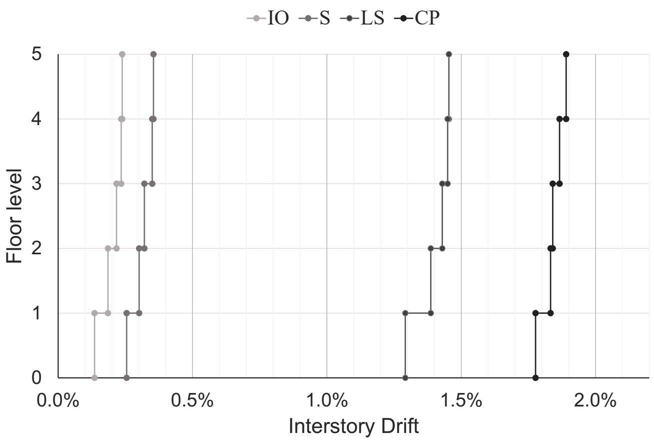

Figure 18. Interstory drift for each limit state.

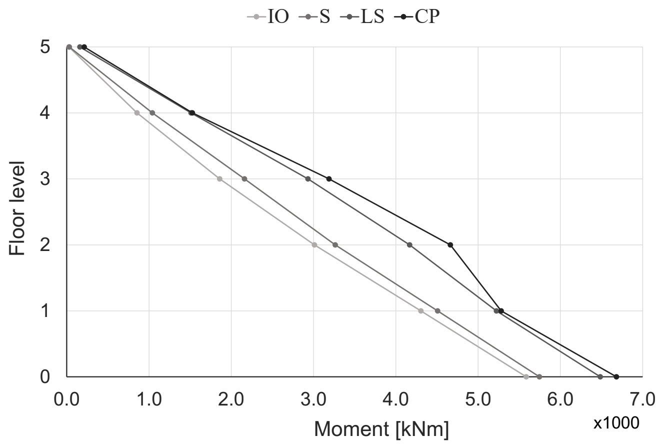

Figure 19. Distribution of bending moment for the hybrid wall for each floor level.

Conclusions

This research provides general indications about the parameters that may influence the design of hybrid walls with unbounded PT walls and supplemental energy dissipation devices in the form of mild reinforcing steel. In particular, a nonlinear system of non-dimensional parametric equations is developed to highlight a rational way to design the PT tendons (area and position) and the mild steel dissipaters (area, position and unbounded length). Recognizing that the proposed system of equations is too complex for design purposes, an extensive sensitivity analysis is conducted to test the dependence of the wall performance on various design parameters: wall aspect ratio, re-centering ability, design drift ratio, non-dimensional axial load and design bending moment.
Starting from the results of the sensitivity analysis, non-dimensional numerical formulas are calibrated for both normalized neutral axis depth and mechanical ratio of the dissipative bars. This allows obtaining a simplified, quick, but still accurate approach for solving the design problem, for each possible combination of the design parameters, in particular, driving the selection and

location of PT tendons and mild steel dissipaters once the bending moment demand and displacement target are known (at this regard, a displacement based design procedure is reported in the appendix). Although extensive parametric analyses have been conducted considering a wide variation of the dimensioning parameters, a comparison with the bounding values reported in ACI ITG-5.1 and ACI ITG-5.2 has been also provided.

The validation of the proposed procedure has been carried out by means of non-linear time history analyses on a selected case study. The procedure provided conservative results and allowed to control the design drift for the life safety limit state. It is recommended to evaluate the performance of the designed wall at the collapse prevention limit state to ensure the suitability of the hybrid system.

Supplemental data

A spreadsheet with the implementation of the proposed procedure is included.

Appendix

This appendix reports a displacement-based design procedure for hybrid walls according to Mpampatsikos (2009). The interested reader is referred to Mpampatsikos (2009) for insights on the derivation of the proposed formulas.

Once the main geometrical features of the hybrid wall and the target design parameter (i.e. the roof drift θ_{top}) have been defined, it is possible to obtain the equivalent elastic single degree of freedom (SDOF) system. This equivalent system represents the nonlinear first mode response of the actual multi degrees of freedom (MDOF) system and it is characterized by the same base shear and work done between SDOF and MDOF. In the first step, the displacement ductility is evaluated as a function of the parameters ν, ζ_u, H_e/B, f_{cm}, μ_M and L_{dad}.

$$\mu_\Delta = \frac{\theta_{top}\left(0.02257+L_{dad}\right)\left[0.09122+\nu\left(0.04483+L_{dad}\right)\right]}{0.123\left(0.04483+L_{dad}\right)\left[\dfrac{0.01463\cdot\theta_{top}}{0.2227+L_{dad}}+\dfrac{f_c^{0.5}\left(0.5327\cdot\mu_M+0.1427\cdot\nu\right)}{1250}\dfrac{H_e}{B}\right]} \qquad \text{(A1)}$$

where the effective height H_e is $(1+2n)/(3n)$ times the wall height, whit n the number of floors, and the normalized axial load ν is:

$$\nu = \frac{N}{A_c\cdot f_{cm}} \qquad \text{(A2)}$$

It is also useful to define the normalized equivalent mass ψ:

$$\psi = \frac{M_e \cdot g}{B \cdot w \cdot f_{cm}} \tag{A3}$$

Subsequently it is possible to calculate the equivalent viscous damping ratio ξ_{eq}:

$$\xi_{eq} = 0.05 + \frac{2.348}{\lambda + 3.901} \frac{\mu_\Delta - 1}{\mu_\Delta \cdot \pi} \tag{A4}$$

Where λ, i.e. re-centering capacity, is a value greater than 1.2. It is worth mentioning that the variability of this factor does not significantly influence the procedure.

Since the proposed procedure is not for tall and slender buildings, it is likely that the equivalent period of the substitute SDOF system (T_e), assessed at design conditions, falls in the region where the displacement response spectrum can be considered to grow linearly with the period. It is possible to calculate the effective period of the substitute SDOF structure $T_{e(A)}$ as:

$$T_{e(A)} = \frac{4\pi^2 \Delta_e \sqrt{0.02 + \xi_{eq}}}{2.5 \cdot a_g \cdot g \cdot S \cdot T_C \sqrt{0.07}} \tag{A5}$$

Where a_g is the peak ground acceleration on rock, T_C is the spectral period corresponding to the end of the constant acceleration region (CEN 2004), S is the site amplification factor and Δ_e is the SDOF design displacement. Δ_e is equal to the total displacement of the MDOF system, Δ_T, times a reduction factor α equal to (1+2*n*)/(3*n*).

It is possible to calculate the effective period of the substitute SDOF structure with another formulation as a function of the normalized base bending moment μ_M (equal to the ratio between the design base moment and the mechanical properties of the section) and the normalized equivalent mass ψ:

$$\mu_M = \frac{M_b}{A_c \cdot f_c \cdot B} \tag{A6}$$

$$T_{e(B)} = 2\pi \sqrt{\frac{\psi \cdot H_f (1+2n) \cdot \theta_{top}}{3g \cdot \mu_M} \frac{H_e}{B}} \tag{A7}$$

Where H_f is the inter-story height (or the average inter-story height). An iterative procedure in terms of μ_M is required to minimize the difference between the results of Eq. A4 and Eq. A5.

Subsequently, starting from T_e (taken as an average between $T_{e(A)}$ and $T_{e(B)}$) and the equivalent damping, it is possible to determine the equivalent mass, stiffness, shear and moment of the equivalent SDOF system:

$$M_e = \frac{\psi \cdot B \cdot \omega \cdot f_c}{g} \tag{A8}$$

$$k_e = (2\pi)^2 \cdot \frac{M_e}{(T_e)^2} \tag{A9}$$

$$V_b = \Delta_e \cdot k_e \tag{A10}$$

$$M_b = V_b \cdot H_e \tag{A11}$$

The described procedure is represented in Figure A1.

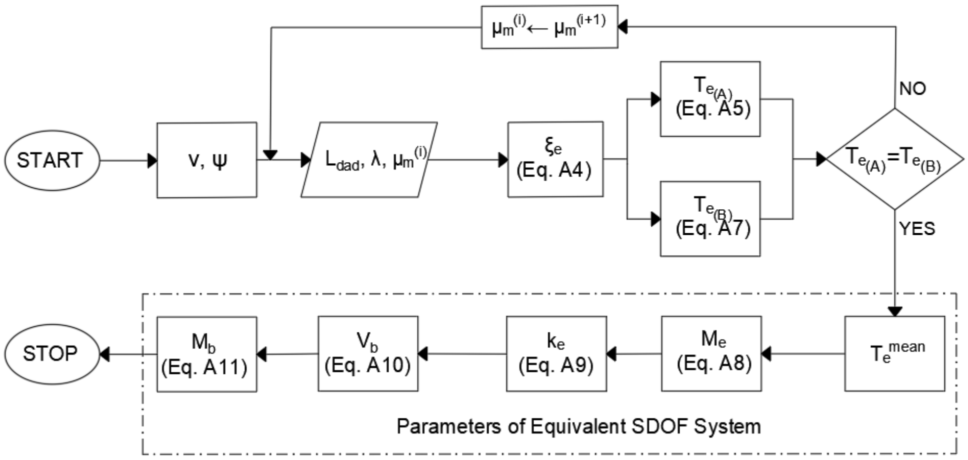

Figure A1. Flow chart for the definition of the equivalent SDOF system.

List of symbols

θ_{top}	Design roof drift
M_b	Design base moment
V_b	Design base shear
H	Total height of the wall
H_f	Inter-story height
B	Base of the wall
w	Width of the wall
H/B	Wall aspect ratio
A_c	Cross-section area of the wall
N	Axial load in the wall
ν	Normalized axial load in the wall
ε_{ccu}	Ultimate strain for confined concrete
ε_{cc0}	Confined concrete strain at "yielding"
f_{cc}	Confined concrete strength
ε_{cu}	Ultimate strain for unconfined concrete
ε_{c0}	Unconfined concrete strain
A_{PT}	Area of the PT tendons
f_c	Unconfined concrete strength

E_C	Elastic modulus of the concrete
E_{PT}	Elastic modulus of the PT tendons
f_{yPT}	Yielding stress of the PT tendons
D_{PT}	Diameter of the PT tendons
L_{PT}	Length of the PT tendons
L_{PTad}	Normalized length of the PT tendons
f_{PT}	Maximum allowed stress for the PT tendons
γ_{PT}	Safety factor for PT tendons
ε_{PT}	Strain in the PT tendons corresponding to pretension
ε_{yPT}	Yielding strain of the PT tendons
ε_{PTad}	Normalized strain of the PT tendons
A_d	Area of the dissipaters
E_d	Elastic modulus of the dissipaters
f_{yd}	Yielding stress of the dissipaters
f_{ud}	Maximum stress of the dissipaters
ε_{yd}	Yielding strain of the dissipaters
ε_{ud}	Ultimate strain of the dissipaters
$\varepsilon_{d,max}$	Maximum design strain of the dissipaters
L_{dad}	Normalized unbounded length of the dissipaters
D_d	Diameter of the dissipaters
μ_M	Normalized base bending moment
μ_D	Displacement ductility
ζ	Normalized neutral axis depth
α, β	Stress block factors
H_T	Total height of the MDOF system
H_e	Equivalent height of the substitute SDOF system
Δ_T	Roof displacement of the MDOF system
Δ_e	Equivalent displacement of the substitute SDOF system
λ	Re-centering capacity
T_C	Period corresponding to the end of the constant acceleration region
S	Soil factor
PGA	Peak ground acceleration with soil amplification
a_g	Peak ground acceleration on rock
γ_j	Stiffness reduction factor
ψ	Normalized equivalent mass
M_T	Total mass of the MDOF system

T_e	Equivalent period of the substitute SDOF system
ξ_{eq}	Equivalent viscous damping ratio of the substitute SDOF system
M_e	Equivalent mass of the substitute SDOF system
K_e	Equivalent stiffness of the substitute SDOF system

References

ACI ITG-5.1. Acceptance Criteria for Special Unbonded Post-Tensioned Precast Structural Walls Based on Validation Testing. ACI Innovation Task Group 5, 2008.

ACI ITG-5.2. Requirements for Design of a Special Unbonded Post-Tensioned Precast Shear Wall Satisfying ACI ITG-5.1. ACI Innovation Task Group 5, 2009.

Ajrab JJ, Pekcan GM, Mander JB. Rocking wall-frame structures with supplemental tendons systems. ACI Structural Journal, 2004; 130 (6):895-903.

Belleri A, Schoettler MJ, Restrepo JI, Fleischman RB. Dynamic behavior of rocking and hybrid cantilever walls in a precast concrete building. ACI Structural Journal, 2014;111 (3):661-671.

Belleri A, Torquati M, Riva P. Finite element modeling of "rocking walls". ECCOMAS Thematic Conference - COMPDYN 2013: 4th International Conference on Computational Methods in Structural Dynamics and Earthquake Engineering, Proceedings - An IACM Special Interest Conference, 2831-2848.

Belleri A. Displacement based design for precast concrete frames with not-emulative connections. Engineering Structures, 2017; 141:228-240.

Smith BJ, Kurama YC, McGinnis MJ. Hybrid precast wall systems for seismic regions. Department of Civil Engineering and Geological Sciences University of Notre Dame, Indiana, 2012.

Brunesi E, Nascimbene R. Extreme response of reinforced concrete buildings through fiber force-based finite element analysis. Engineering Structures, 2014; 69:206-15.

Buddika HADS, Wijeyewickrema AC. Seismic Performance Evaluation of Posttensioned Hybrid Precast Wall-Frame Buildings and Comparison with Shear Wall-Frame Buildings. Journal of Structural Engineering, 2016; 142(6): 04016021.

Casotto C, Silva V, Crowley H, Nascimbene R, Pinho R. Seismic fragility of Italian RC precast industrial structures. Engineering Structures, 2015; 94:122-136.

CEN 2004 Eurocode 8, Design of structures for earthquake resistance - Part 1: General rules, seismic actions and rules for buildings. European Standard, Brussels, Belgium, 2004.

Cimellaro GP, Reinhorn AM, Bruneau M. Framework for analytical quantification of disaster resilience. Engineering Structures, 2010; 32(11):3639-3649.

Crisafulli FJ, Restrepo J I, Park R. Seismic design of lightly reinforced precast rectangular wall panels. PCI Journal, 2002; 47(4):104–12.

Fronteddu L, Léger P, Tinawi R. Static and dynamic behavior of concrete lift joint interfaces. Journal of Earthquake Engineering, 1998;124(12):1418–1430.

Golzar FG, Rodgers GW, Chase JG. Nonlinear spectral design analysis of a structure for hybrid self-centring device enabled structures. Structural Engineering and Mechanics, 2017; 61(6):701-709.

Golzar FG, Rodgers GW, Chase JG. Design and Experimental Validation of a Re-centring Viscous Dissipater. Engineering Structures, 2018; 13:193-200.

Hamid NH, Mander JB. Lateral seismic performance of multipanel precast hollowcore walls. Journal of Structural Engineering, 2010; 136(7):795-804.

Hamid NH, Mander JB. Damage avoidance design for buildings. Journal of Civil Engineering, 2014; 18(2):541-548.

Holden T, Restrepo J, Mander JB. Seismic performance of precast reinforced and prestressed concrete walls. Journal of Structural Engineering, 2003; 129(3):286-296.

Kurama YC. Seismic design of unbonded post-tensioned precast concrete walls with supplemental viscous damping. ACI Structural Journal, 2000; 97(4):648-658.

Kurama YC. Seismic Design of Partially Post-Tensioned Precast Concrete Walls. PCI Journal, 2005; 50(4):100-125.

Kurama YC, Pessiki S, Sause R, Lu WL. Lateral load behaviour and seismic design of unbonded post-tensioned precast concrete walls. PCI Journal, 1999; 46(4):622-633.

Kurama YC, Pessiki S, Sause R, Lu L, El-Sheikh MT. Analytical Modelling and Lateral Load Behavior of Unbonded Post-Tensioned Precast Concrete Walls. 1998a, Lehigh University.

Kurama YC, Sause R, Pessiki S, Lu L, El-Sheikh MT. Seismic Design and Response Evaluation of Unbonded Post-Tensioned Precast Concrete Walls. 1998b, Lehigh University.

Kurama YC. Hybrid Post-Tensioned Precast Concrete Walls for Use in Seismic Regions. PCI Journal, 2002; 47(5):36-59.

Mander JB, Priestley MJN, Park R. Theoretical stress-strain model for confined concrete. Journal of Structural Engineering ASCE, 1988; 114(8):1804-1826.

Mander JB, Cheng CT. Seismic resistance of bridge piers based on damage avoidance design. Department of Civil, Structural and Environment Engineering, Technical Report NCEER 1997.

Mansour N, Shen Y, Christopoulos C, Tremblay R. Experimental evaluation of nonlinear replaceable links in eccentrically braced frames and moment resisting frames. 14th World Conference on Earthquake Engineering, 2008.

Marriott D, Pampanin S, Bull D, Palermo A. Dynamic Testing of Precast, Post- Tensioned Rocking Walls Systems with Alternative Dissipating Solutions. Bulletin of the New Zealand Society for Earthquake Engineering, 2008; 41(2):90-103.

Marriott D, Pampanin S, Palermo A. Biaxial testing of unbonded post-tensioned rocking bridge piers with external replacable dissipaters. Earthquake Engineering and Structural Dynamics, 2011; 40:1723-1741.

MidasGEN 2017, MIDAS Information Technologies Co. Ltd.

Mpampatsikos V. DDBD of rocking walls with mild steel dissipaters. Ph.D. dissertation, 2009; ROSE School, IUSS, Pavia, Italy.

Mpampatsikos V, Bolognini D, Nascimbene R. Assessment of the equivalent viscous damping ratio for hybrid wall-to-foundation connections of precast wall panels. Compdyn, 2009, Rhodes, Greece.

Nascimbene R. Numerical model of a reinforced concrete building: Earthquake analysis and experimental validation. Periodica Polytechnica: Civil Engineering, 2015; 59 (4):521-530.

Nazari M, Sritharan S, Aaleti S. Single precast concrete rocking walls as earthquake force-resisting elements. Earthquake Engineering and Structural Dynamics, 2017; 46:753-769.

OpenSees – Open System for Earthquake Engineering Simulation Pacific Earthquake Engineering Research Center – Version 2.1.0., 2009, University Ave. Berkeley, CA.

Pampanin S, Priestley MJN, Sritharan S. Analytical modeling of the seismic behaviour of precast concrete frames designed with ductile connections. Journal of Earthquake Engineering, 2001; 5(3):329-367.

Paulay T, Priestley MJN. Seismic design of reinforced concrete and masonry buildings, 1992, Wiley, New York.

Pennucci D, Calvi GM, Sullivan T. Displacement based design of precast walls with additional dampers. Journal of Earthquake Engineering, 2009; 13(S1):40-65.

Pérez FJ, Pessiki S, Sause R, Lu LW. Lateral load tests of unbonded post-tensioned precast concrete walls. Special publication of large-scale structural testing, 2003, Paper No. SP 211-8, American Concrete Institute, Detroit, 161–182.

Priestley MJN. The PRESSS Program – Current status and proposed planes for Phase III. PCI Journal 1996; 41(2):22-40.

Priestley MJN, Calvi GM, Kowalsky MJ. Displacement based seismic design of structures, 2007, IUSS Press Ed., Pavia.

Priestley MJN, Sritharan S, Conley JR, Pampanin S. Preliminary results and conclusions from the PRESSS five-storey precast concrete test buildings. PCI Journal, 1999; 44(6):42-67.

Priestley MJN, Tao JR. Seismic response of precast prestressed concrete frames with partially debonded tendons. PCI Journal, 1993; 38(1):58-69.

Qureshi IM, Warnitchai P. Computer modeling of dynamic behavior of rocking wall structures including the impact-related effects. Advances in Structural Engineering, 2016; 19(8):1245-1261

Restrepo JI, Rahman A. Seismic performance of self-centering structural walls incorporating energy dissipaters. J Struct Eng 2007; 133, SPECIAL ISSUE: Precast-Prestreesed Concrete Structures under Natural and Human-Made Hazards, 1560–1570.

REDI Rating System. Resilience-based Earthquake Design Initiative for the next generation of buildings 2013.

Rodgers GW, Chase JG, Mander J, Dhakal RP, Solberg KM. DAD Post-Tensioned Concrete Connections with Lead Dampers: Analytical Models and Experimental Validation. 8th Pacific Conference on Earthquake Engineering 2007.

Rodgers GW, Solberg KM, Chase JG, Mander JB, Bradley BA, Dhakal RP, Li L. Performance of a damage-protected beam–column subassembly utilizing external HF2V energy dissipation devices. Earthquake Engineering & Structural Dynamics, 2008; 37:1549-1564.

SeismoStruct - A computer programme for static and dynamic nonlinear analysis of frames structures, SeismoSoft; Italy, 2015.

Shibata A, Sozen M. Substitute structure method for seismic design in reinforced concrete. Journal Structural Division ASCE, 1976; 102(12):3548-3566.

Schoettler MJ, Belleri A, Zhang D, Restrepo JI, Fleischman RB. Preliminary results of the shake-table testing for the development of a diaphragm seismic design methodology, PCI Journal, 2009; 54(1)100-124.

Spacone E, Filippou FC, Taucer FF. Fibre beam-column model for non-linear analysis of RC frames: Part I. Formulation. Earthquake Engineering & Structural Dynamics, 1996; 25:711-25.

Toranzo LA, Restrepo JI, Mander JB, Carr AJ. Shake-Table Tests of Confined-Masonry Rocking Walls with Supplementary Hysteretic Damping, Journal of Earthquake Engineering, 2009; 13(6):882-898.

Twigden KM, Sritharan S, Henry RS. Cyclic testing of unbonded post-tensioned concrete wall systems with and without supplemental damping. Engineering Structures, 2017; 140:406-420.

Twigden KM, Henry RS. Shake table testing of unbonded post-tensioned concrete walls with and without additional energy dissipation. Soils Dynamics and Earthquake Engineering, 2019; 119:375-389.

Venmarcke EH, Gasparini DA. Simulated earthquake motions compatible with prescribed response spectra—SIMQKE-1. M.I.T. Department of Civil Engineering Research Report R76-4; 1976.

Wiebe L, Christopoulos C. Mitigation of Higher Mode Effects in Base-Rocking Systems by Using Multiple Rocking Sections. Journal Of Earthquake Engineering, 2009; 13(Sup1):83-108.

Yin Z, Feng D, Yang W. Damage Analyses of Replaceable Links in Eccentrically Braced Frame (EBF) Subject to Cyclic Loading. Journal of Applied Sciences, 2019; 9(2), 332.